Received: Added at production | Revised: Added at production | Accepted: Added at production

DOI: xxx/xxxx

SCIENTIFIC ARTICLE

An adaptive projection-based model reduction method for nonlinear mechanics with internal variables: application to thermo-hydro-mechanical systems.

Angelo Iollo[1,2] | Giulia Sambataro*[1,2] | Tommaso Taddei[1,2]

[1]IMB, UMR 5251, Univ. Bordeaux, 33400, Talence, France
[2]INRIA, Inria Bordeaux Sud-Ouest, Team MEMPHIS, 33400, Talence, France

Correspondence
*Giulia Sambataro. Email: giulia.sambataro@inria.fr

Abstract

We propose a projection-based monolithic model order reduction (MOR) procedure for a class of problems in nonlinear mechanics with internal variables. The work is is motivated by applications to thermo-hydro-mechanical (THM) systems for radioactive waste disposal. THM equations model the behaviour of temperature, pore water pressure and solid displacement in the neighborhood of geological repositories, which contain radioactive waste and are responsible for a significant thermal flux towards the Earth's surface. We develop an adaptive sampling strategy based on the POD-Greedy method, and we develop an element-wise empirical quadrature hyper-reduction procedure to reduce assembling costs. We present numerical results for a two-dimensional THM system to illustrate and validate the proposed methodology.

KEYWORDS:
parameterized partial differential equations; model order reduction; nonlinear mechanics

1 | INTRODUCTION

1.1 | Model reduction for a class of models in nonlinear mechanics

The disposal and storage of high-level radioactive waste materials in geological means requires a careful assessment of the long-term effects on neighboring areas. The system behaviour is well-described by time-dependent large-scales coupled systems of partial differential equations (PDEs), which take into account the thermal, hydraulic and mechanical response of the geological medium. Numerical simulation of these systems is challenging due to several difficulties: first, finite element (FE) models of the problem are highly-nonlinear, time-dependent and high-dimensional; second, due to the uncertainty in model parameters, we need to solve the model for many different system configurations (*many-query* problem). In this work, we shall devise a model-order reduction (MOR) strategy to speed up parametric studies for radioactive waste disposal applications.

In this contribution we study a general class of nonlinear problems in structural mechanics with internal variables. We consider the spatial variable x in the Lipschitz domain $\Omega \subset \mathbb{R}^d$ with $d = 2, 3$, and the time variable t in the time internal $(0, T_f)$, where T_f is the final time. We further define the vector of parameters μ in the compact parameter region $\mathcal{P} \subset \mathbb{R}^P$. We introduce the state (or primary) variables $\underline{U}$ and internal (or dependent) variables $\underline{W}$; we denote by $\mathcal{X}$ and $\mathcal{W}$ suitable Hilbert spaces in Ω for $\underline{U}$ and $\underline{W}$, and we define the space of continuous functions from $(0, T_f)$ to $\mathcal{X}$ and $\mathcal{W}$, $C(0, T_f; \mathcal{X})$ and $C(0, T_f; \mathcal{W})$. Then, we

introduce the parameterised problem of interest: given $\mu \in \mathcal{P}$, find $(\underline{U}_\mu, \underline{W}_\mu) \in C(0, T_\mathrm{f}; \mathcal{X}) \times C(0, T_\mathrm{f}; \mathcal{W})$ such that

$$\begin{cases} \mathcal{G}_\mu(\underline{U}_\mu, \partial_t \underline{U}_\mu, \underline{W}_\mu) = 0 \ \text{ in } \Omega \times (0, T_\mathrm{f}) \\ \dot{\underline{W}}_\mu = \mathcal{F}_\mu(\underline{U}_\mu, \underline{W}_\mu), \quad \text{ in } \Omega \times (0, T_\mathrm{f}) \end{cases} \tag{1}$$

with suitable initial and boundary conditions. Here, $\mathcal{G}_\mu$ is a nonlinear second-order in space, first-order in time differential operator that is associated with the equilibrium equations, while $\mathcal{F}_\mu$ is a set of ordinary differential equations (ODEs) that is associated with the constitutive laws.

Our methodology is motivated by the application to thermo-hydro-mechanical (THM) systems of the form (1), which are widely used to model the system's response for radioactive waste disposal applications. Radioactive material is placed in an array of horizontal boreholes (dubbed *alveoli*) deep underground: due to the large temperature of the alveoli, a thermal flux is generated; the thermal flux then drives the mechanical and hydraulic response of the medium over the course of several years. We refer to section 4 for a detailed discussion of the considered THM model and boundary conditions.

1.2 | Objective of the work and relationship to previous works

We propose a projection-based monolithic model order reduction (MOR[1,2,3]) technique for problems of the form (1), with particular emphasis on THM systems. The approach is characterised by an offline/online splitting to reduce the marginal cost, and relies on Galerkin projection to devise a reduced-order model (ROM) for the solution coefficients. We rely on hyper-reduction to speed up the assembly of the ROM during the online stage, and we rely on adaptive sampling to reduce the offline training costs.

The contribution of this work is the development of a POD-Greedy technique for coupled problems with internal variables. First, we present a time-average *a posteriori* error indicator and compare it with a more standard discrete $L^2(0, T_\mathrm{f}; \mathcal{X}')$ dual residual in terms of computational and memory costs and effectivity. This is crucial for the efficiency of the adaptive method. Second, we apply a greedy sampling (based on the proposed error indicator) to effectively explore the parameter domain. Third, we introduce in this framework a hyper-reduction technique based on an element-wise empirical quadrature (EQ) procedure.

EQ procedures also dubbed mesh sampling and weighting have been first proposed in Refs.[4,5,6] and further developed in several other works including Ref.[7]: the key feature of EQ is to recast the problem of hyper-reduction as a sparse representation problem and then resort to state-of-the-art techniques in machine learning and signal processing to estimate the solution to the resulting optimisation problem. Here, we rely on the approach employed in Ref.[8], which combines the methods in Refs.[4,5] and relies on non-negative least-squares to estimate the solution to the sparse representation problem.

As discussed in section 3, the presence of internal variables requires several changes to the EQ approach in Ref.[8]. Our approach relies on a different treatment of primary and internal variables compared to the works in Ref.[9,10], as explained in section 3.2. In addition, in the present work we aim at solving coupled systems that model the interaction between mechanic, thermal and hydraulic response, as described in section 4. In section 3 we clarify to what extent the management of internal variables requires a careful adaptation of the MOR technique illustrated in Ref.[8] and we briefly compare our treatment of internal variables with Refs.[9,10].

We emphasise that several other hyper-reduction techniques have been proposed in the literature including the empirical interpolation method (EIM[11]) and its discrete variant[12], the approach in Ref.[13], and Gappy-POD[14,15]. We also refer to Refs.[16,17] for further empirical (or reduced) quadrature procedures for problems in nonlinear mechanics. A thorough comparison of state-of-the-art hyper-reduction techniques is beyond the scope of this work.

The POD-Greedy algorithm was introduced in Ref.[18] and analysed in Ref.[19]: the approach combines proper orthogonal decomposition (POD[20,21,22]) to compress temporal trajectories with a greedy search driven by an error indicator to explore the parameter domain. In this work, similarly to Ref.[23], we rely on a time-averaged error indicator to drive the greedy search; furthermore, we test two different compression strategies to update the POD basis at each greedy iteration.

We further observe that the development of online-efficient adaptive ROMs for problems of the form (1) is extremely limited in the literature. Relevant examples include the works in Refs.[13,24,25], which, however, do not consider adaptive sampling. As regards the application of MOR to THM systems, we recall the recent contribution by Larion *et al.*[26]: note, however, that the work in Ref.[26] deals with a linearised THM model without internal variables.

1.3 | Outline

The outline of this paper is the following. In section 2 we briefly present the mathematical model and the numerical discretisation for the general class of nonlinear problems in structural mechanics defined in (1). In section 3, we present the MOR technique: to simplify the presentation, we first discuss the solution reproduction problem and then we extend the approach to the parametric case. Section 4 contains details of the THM mathematical model considered in the numerical section. In section 5, we present extensive numerical investigations for a two-dimensional THM system. In section 6, we draw some conclusions and we outline a number of subjects of ongoing research.

2 | FORMULATION

2.1 | Notation

In this section, we omit dependence on the parameter. Given $\Omega \subset \mathbb{R}^d$, we define the triangulation $\{\mathtt{D}_k\}_{k=1}^{N_\mathrm{e}}$, where N_e denotes the total number of elements, the nodes $\{x_j^{\mathrm{hf}}\}_{j=1}^{\mathcal{N}}$ and the connectivity matrix $\mathtt{T} \in \mathbb{N}^{N_\mathrm{e}, n_\mathrm{lp}}$ such that $\mathtt{T}_{k,i} \in \{1, \dots, \mathcal{N}\}$ is the index of the i-th node of the k-th element of the mesh and n_lp is the number of degrees of freedom in each element. We remark that throughout the paper the acronym HF stands for high-fidelity discretisation.

Then, we introduce the continuous Lagrangian FE basis $\{\varphi_i\}_{i=1}^{\mathcal{N}}$ associated with the triangulation $\{\mathtt{D}_k\}_{k=1}^{N_\mathrm{e}}$, such that $\varphi_i(x_j^{\mathrm{hf}}) = \delta_{i,j}$, and we introduce the FE space for the state variables:

$$\mathcal{X}_{\mathrm{hf}} := \mathrm{span}\left\{ \varphi_i \underline{e}_j \; : \quad i = 1, \dots, \mathcal{N}, \quad j = 1, \dots, D_{\mathrm{eq}} \right\}, \tag{2}$$

where $\underline{e}_1, \dots, \underline{e}_{D_{\mathrm{eq}}}$ are the elements of the canonical basis and D_{eq} is the number of state variables. We define the state variables for the specific problem of interest in in section 4.1.

We denote by $\|\cdot\| = \sqrt{(\cdot,\cdot)}$ the norm of $\mathcal{X}_{\mathrm{hf}}$; furthermore, given $\underline{u} \in \mathcal{X}_{\mathrm{hf}}$, we denote by $\underline{\mathbf{u}} \in \mathbb{R}^{\mathcal{N}, D_{\mathrm{eq}}}$ the corresponding vector (or matrix) of coefficients such that $(\underline{\mathbf{u}})_{j,\ell} = \left(\underline{u}(x_j^{\mathrm{hf}})\right)_\ell$ for $j = 1, \dots, \mathcal{N}$ and $\ell = 1, \dots, D_{\mathrm{eq}}$; notation $\underline{\mathbf{u}}(:, \ell)$ refers to the ℓ^{th} column of the matrix $\underline{\mathbf{u}}$.

In view of the MOR formulation, we introduce the elemental restriction operators $\mathbf{E}_k : \mathbb{R}^{\mathcal{N}} \to \mathbb{R}^{n_\mathrm{lp}}$ such that

$$\left(\mathbf{E}_k \underline{\mathbf{u}}\right)_{i,\ell} = \left(\underline{u}(x^{\mathrm{hf}}_{\mathtt{T}_{k,i}})\right)_\ell, \quad i = 1, \dots, n_\mathrm{lp}, \; \ell = 1, \dots, D_{\mathrm{eq}}, \; k = 1, \dots, N_\mathrm{e}. \tag{3a}$$

Furthermore, we introduce the quadrature points $\{x^{\mathrm{hf,q}}_{q,k}\}_{q,k} \subset \Omega$, such that $x^{\mathrm{hf,q}}_{q,k}$ is the q-th quadrature point of the k-th element of the mesh, with $q = 1, \dots, n_\mathrm{q}$, and the operators $\mathbf{E}_k^{\mathrm{qd}} : \mathbb{R}^{\mathcal{N}} \to \mathbb{R}^{n_\mathrm{q}}$ and $\mathbf{E}_k^{\mathrm{qd},\nabla} : \mathbb{R}^{\mathcal{N}} \to \mathbb{R}^{n_\mathrm{q}, d}$ such that

$$\left(\mathbf{E}_k^{\mathrm{qd}} \underline{\mathbf{u}}\right)_{q,\ell} = \left(\underline{u}(x^{\mathrm{hf,q}}_{q,k})\right)_\ell, \quad \left(\mathbf{E}_k^{\mathrm{qd},\nabla} \underline{\mathbf{u}}\right)_{q,\ell,j} = \left(\frac{\partial}{\partial x_j} \underline{u}(x^{\mathrm{hf,q}}_{q,k})\right)_\ell \tag{3b}$$

where $q = 1, \dots, n_\mathrm{q}$, $\ell = 1, \dots, D_{\mathrm{eq}}$, $k = 1, \dots, N_\mathrm{e}$ and $j = 1, \dots, d$. To shorten notation, in the following, we further define $\mathbf{E}_k^{\mathrm{qd},\star} : \mathbb{R}^{\mathcal{N}} \to \mathbb{R}^{n_\mathrm{q}, d+1}$ such that

$$\left(\mathbf{E}_k^{\mathrm{qd},\star} \underline{\mathbf{u}}\right)_{q,\ell,1} = \left(\mathbf{E}_k^{\mathrm{qd}} \underline{\mathbf{u}}\right)_{q,\ell}, \quad \left(\mathbf{E}_k^{\mathrm{qd},\star} \underline{\mathbf{u}}\right)_{q,\ell,2\dots,d+1} = \left(\mathbf{E}_k^{\mathrm{qd},\nabla} \underline{\mathbf{u}}\right)_{q,\ell,\cdot}. \tag{3c}$$

Remark 1. For the THM problem considered in this work, the state $\underline{U}$ contains the displacement $\underline{u}$, the water pressure p and the temperature T ($D_{\mathrm{eq}} = 2 + d$); as discussed in Ref.[27], to avoid instabilities, it is important to use polynomials of degree κ for displacement and $\kappa - 1$ for pressure and temperature: as a result, we should introduce separate restriction operators and separate FE spaces for the different components of the state. In the main body of the paper we choose to not explicitly address this issue to simplify notation: we remark that the extension to κ-$(\kappa - 1)$ discretisations is computationally tedious but methodologically straightforward.

2.2 | Finite element discretisation of (1)

We introduce the time grid $0 = t^{(0)} < t^{(1)} < \dots < t^{(J_{\max})} = T_\mathrm{f}$ such that $t^{(j)} = j\Delta t$. We denote by $\{\underline{U}^{(j)}_{\mathrm{hf}}\}_{j=1}^{J_{\max}} \subset \mathcal{X}_{\mathrm{hf}}$ the FE approximation of the state variables at all times, that is, the ℓ^{th} column of $\underline{U}^{(j)}_{\mathrm{hf}}$ is the approximation of the ℓ^{th} state variable at time $t^{(j)}$. On the other hand, we denote by $\underline{\mathbf{W}}^{(j)}_{\mathrm{hf}} \in \mathbb{R}^{n_\mathrm{q}, N_\mathrm{e}, D_{\mathrm{int}}}$ the tensor associated with the evaluation of the internal variables

at time $t^{(j)}$ in the quadrature points:

$$\left(\underline{\mathbf{W}}_{\mathrm{hf}}^{(j)}\right)_{q,k,\ell} = \left(\underline{W}_{\mathrm{hf}}^{(j)}(x_{q,k}^{\mathrm{hf,q}})\right)_{\ell}, \quad q = 1,\dots,n_{\mathrm{q}},\ k = 1,\dots,N_{\mathrm{e}},\ \ell = 1,\dots,D_{\mathrm{int}}.$$

Given $\ell \in \{1,\dots,D_{\mathrm{eq}}\}$, we further denote by $\mathtt{I}_{\mathrm{dir}}^{\ell} \subset \{1,\dots,N_{\mathrm{hf}}\}$ the indices associated with Dirichlet boundary conditions (if any) of the ℓ^{th} state component, and we denote by $\underline{\mathbf{g}}_{\mathrm{dir},\ell}^{(j)} \in \mathbb{R}^{|\mathtt{I}_{\mathrm{dir}}^{\ell}|}$ the vector that contains the value of the ℓ^{th} state component at each Dirichlet node at time $t^{(j)}$.

We state the FE discretisation of (1) as follows: for $j = 1, 2, \dots$, find $(\underline{U}_{\mathrm{hf}}^{(j)}, \underline{W}_{\mathrm{hf}}^{(j)})$ such that

$$\begin{cases} \mathcal{R}^{\mathrm{hf}}\left(\underline{\mathbf{U}}_{\mathrm{hf}}^{(j)},\ \underline{\mathbf{U}}_{\mathrm{hf}}^{(j-1)},\ \underline{\mathbf{W}}_{\mathrm{hf}}^{(j)},\ \underline{\mathbf{W}}_{\mathrm{hf}}^{(j-1)},\ \underline{\mathbf{V}}\right) = 0, \quad \forall\, \underline{V} \in \mathcal{X}_{\mathrm{hf},0}; \\ \underline{\mathbf{U}}_{\mathrm{hf}}^{(j)}(\mathtt{I}_{\mathrm{dir}}^{\ell}, \ell) = \underline{\mathbf{g}}_{\mathrm{dir},\ell}^{(j)}, \quad \ell = 1,\dots,D_{\mathrm{eq}}; \\ \left(\underline{\mathbf{W}}_{\mathrm{hf}}^{(j)}\right)_{q,k,\ell} = \mathcal{F}_{\ell}^{\mathrm{hf}}\left(\left(\mathbf{E}_k^{\mathrm{qd},\star}\underline{\mathbf{U}}_{\mathrm{hf}}^{(j)}\right)_{q,\cdot},\ \left(\mathbf{E}_k^{\mathrm{qd},\star}\underline{\mathbf{U}}_{\mathrm{hf}}^{(j-1)}\right)_{q,\cdot},\ \left(\underline{\mathbf{W}}_{\mathrm{hf}}^{(j-1)}\right)_{q,k,\cdot}\right), \\ \qquad\qquad q = 1,\dots,n_{\mathrm{q}}, k = 1,\dots,N_{\mathrm{e}}, \ell = 1,\dots,D_{\mathrm{int}}. \end{cases} \tag{4}$$

where $\mathcal{X}_{\mathrm{hf},0} := \{\underline{V} \in \mathcal{X}_{\mathrm{hf}} \ :\ \underline{\mathbf{V}}(\mathtt{I}_{\mathrm{dir}}^{\ell}, \ell) = 0, \ell = 1,\dots,D_{\mathrm{eq}}\}$ is the test space for all state equations. Note that $\mathcal{R}^{\mathrm{hf}}$ and $\underline{\mathcal{F}}^{\mathrm{hf}}$ are the discrete counterparts of the operators $\mathcal{G}$ and $\underline{\mathcal{F}}$ in (1). Note also that the constitutive laws are stated in the quadrature points of the mesh and the internal fields should be computed in the quadrature points of the mesh. Dirichlet boundary conditions are imposed via a lifting; Neumann boundary conditions are introduced in the weak formulation associated to the first equation in system (4) via the Green's formula. We refer to section 4 for the particular form of problem (4) associated to THM systems.

The underlying problem is second-order in space and first-order in time. At each time step, following Ref.[27], we solve (4) for $\underline{U}_{\mathrm{hf}}^{(j)}$ using a Newton method with line search; the method requires the computation of the Jacobian and the solution to a coupled linear system of size $\mathcal{N} \cdot D_{\mathrm{eq}}$.

In view of the introduction of the MOR methodology, in particular the hyper-reduction procedure, we write the residual $\mathcal{R}^{\mathrm{hf}}$ as the sum of local contributions.

$$\begin{aligned} &\mathcal{R}^{\mathrm{hf}}\left(\underline{\mathbf{U}}^{(j)},\ \underline{\mathbf{U}}^{(j-1)},\ \underline{\mathbf{W}}^{(j)},\ \underline{\mathbf{W}}^{(j-1)},\ \underline{\mathbf{V}}\right) = \\ &\sum_{k=1}^{N_{\mathrm{e}}} r_k^{\mathrm{hf}}\left(\mathbf{E}_k\underline{\mathbf{U}}^{(j)},\ \mathbf{E}_k\underline{\mathbf{U}}^{(j-1)},\ \left(\underline{\mathbf{W}}^{(j)}\right)_{\cdot,k,\cdot},\ \left(\underline{\mathbf{W}}^{(j-1)}\right)_{\cdot,k,\cdot},\ \mathbf{E}_k\underline{\mathbf{V}}^{(j)}\right) \end{aligned} \tag{5}$$

As explained in section 3, this decomposition provides the foundation of our hyper-reduction procedure.

3 | METHODOLOGY

We propose a time-marching Galerkin ROM based on linear approximations. More precisely, we consider approximations of the form

$$\widehat{\underline{U}}_{\mu}^{(j)} = \underline{Z}\,\widehat{\boldsymbol{\alpha}}_{\mu}^{(j)} = \sum_{n=1}^{N}\left(\widehat{\boldsymbol{\alpha}}_{\mu}^{(j)}\right)_n \underline{\zeta}_n, \quad j = 1,\dots,J_{\max}, \tag{6}$$

where $\{\widehat{\boldsymbol{\alpha}}_{\mu}^{(j)}\}_{j=1}^{J_{\max}} \subset \mathbb{R}^N$ are referred to as solution coefficients and are computed by solving a suitable ROM, while $\underline{Z} : \mathbb{R}^N \to \mathcal{X}_{\mathrm{hf}}$ is the reduced-order basis (ROB) and $\mathcal{Z} := \mathrm{span}\{\underline{\zeta}_n\}_{n=1}^{N}$ is the reduced space. In presence of non-homogeneous Dirichlet conditions, it is convenient to consider affine approximations of the form $\widehat{\underline{U}}_{\mu}^{(j)} = \underline{H}\mathbf{g}^{(j)} + \underline{Z}\,\widehat{\boldsymbol{\alpha}}_{\mu}^{(j)}$, where $\underline{H}$ is a suitable lifting operator (see, e.g., Ref.[8]) and $\mathcal{Z} \subset \mathcal{X}_{\mathrm{hf},0}$: since in this work, we consider homogeneous Dirichlet conditions, we do not address the treatment of non-homogeneous conditions. We consider a single reduced basis $\underline{Z}$ for all state variables in $\{\underline{U}_{\mathrm{hf}}^{(j)}\}_{j=1}^{J_{\max}}$; we discuss the choice of the inner product in section 4 (cf. Eq. (33)).

The Galerkin ROM is obtained by projecting (4) onto the reduced space $\mathcal{Z}$: this leads to a nonlinear system of N equations at each time step. To reduce assembly costs, it is important to avoid integration over the whole integration domain. Towards this

Algorithm 1 Solution reproduction problem: offline/online decomposition

Offline stage:

1: compute $\{\underline{\mathbf{U}}^{(j)}_{\mathrm{hf},\mu}\}_{j\in \mathtt{I}_\mathrm{s}}$, $\mathtt{I}_\mathrm{s} \subset \{1,\dots,J_{\max}\}$;

2: construct the ROB $\underline{Z}$; ▷ section 3.1.1

3: construct the weights $\boldsymbol{\rho}^{\mathrm{eq}}$. ▷ section 3.1.2

Online stage:

4: compute $\{\widehat{\boldsymbol{\alpha}}^{(j)}_\mu\}_{j=1}^{J_{\max}}$ by solving the ROM (7).

end, we define the indices associated with the "sampled elements" $\mathtt{I}_{\mathrm{eq}} \subset \{1,\dots,N_\mathrm{e}\}$ and we define the EQ residual:

$$\begin{aligned}&\mathcal{R}^{\mathrm{eq}}_\mu\left(\underline{\mathbf{U}}^{(j)},\, \underline{\mathbf{U}}^{(j-1)},\, \underline{\mathbf{W}}^{(j)},\, \underline{\mathbf{W}}^{(j-1)},\, \underline{\mathbf{V}}\right) = \\ &\sum_{k\in\mathtt{I}_{\mathrm{eq}}} \rho^{\mathrm{eq}}_k\, r^{\mathrm{hf}}_{\mu,k}\left(\mathbf{E}_k\underline{\mathbf{U}}^{(j)},\, \mathbf{E}_k\underline{\mathbf{U}}^{(j-1)},\, \left(\underline{\mathbf{W}}^{(j)}\right)_{\cdot,k,\cdot},\, \left(\underline{\mathbf{W}}^{(j-1)}\right)_{\cdot,k,\cdot},\, \mathbf{E}_k\underline{\mathbf{V}}^{(j)}\right)\end{aligned} \tag{7a}$$

where $\boldsymbol{\rho}^{\mathrm{eq}} = [\rho^{\mathrm{eq}}_1, ..., \rho^{\mathrm{eq}}_{N_\mathrm{e}}]^T$ is a sparse vector of positive weights such that $\rho^{\mathrm{eq}}_k = 0$ if $k \notin \mathtt{I}_{\mathrm{eq}}$. In conclusion, the Galerkin ROM reads as follows: for $j = 1, 2, \dots$, find $(\underline{\widehat{U}}^{(j)}_\mu, \underline{\widehat{W}}^{(j)}_\mu)$ such that

$$\begin{cases}\mathcal{R}^{\mathrm{eq}}_\mu\left(\underline{\widehat{\mathbf{U}}}^{(j)}_\mu,\, \underline{\widehat{\mathbf{U}}}^{(j-1)}_\mu,\, \underline{\widehat{\mathbf{W}}}^{(j)}_\mu,\, \underline{\widehat{\mathbf{W}}}^{(j-1)}_\mu,\, \underline{\mathbf{V}}\right) = 0, \quad \forall\, \underline{V} \in \mathcal{Z};\\ \left(\underline{\widehat{\mathbf{W}}}^{(j)}_\mu\right)_{q,k,\ell} = \mathcal{F}^{\mathrm{hf}}_{\mu,\ell}\left(\left(\mathbf{E}^{\mathrm{qd},\star}_k\underline{\widehat{\mathbf{U}}}^{(j)}_\mu\right)_{q,\cdot},\, \left(\mathbf{E}^{\mathrm{qd},\star}_k\underline{\widehat{\mathbf{U}}}^{(j-1)}_\mu\right)_{q,\cdot},\, \left(\underline{\widehat{\mathbf{W}}}^{(j-1)}_\mu\right)_{q,k,\cdot}\right),\\ \qquad\qquad q = 1,\dots,n_\mathrm{q}, k \in \mathtt{I}_{\mathrm{eq}}, \ell = 1,\dots,D_{\mathrm{int}}.\end{cases} \tag{7b}$$

Note that the internal variables need to be computed only in the sampled elements. Furthermore, computation of (7b) only requires the storage of the ROB in the sampled elements, $\{\mathbf{E}_k\underline{\boldsymbol{\zeta}}_n : n = 1,\dots,N, k \in \mathtt{I}_{\mathrm{eq}}\}$: provided that $|\mathtt{I}_{\mathrm{eq}}| \ll N_\mathrm{e}$, this leads to significant savings in terms of online assembly costs and also in terms of online memory costs.

In the remainder of this section, we shall discuss the construction of the ROB $\underline{Z}$ (*data compression*), the empirical quadrature rule $\boldsymbol{\rho}^{\mathrm{eq}}$ (*hyper-reduction*) and also the error indicator. To simplify the presentation, in section 3.1 we focus on the solution reproduction problem, while in section 3.2 we discuss the extension to the parametric problem.

3.1 | Solution reproduction problem

The solution reproduction problem refers to the task of reproducing the results obtained for a fixed value of the parameter μ. Algorithm 1 summarises the procedure: during the offline stage, we compute the HF solution to (6) for a given parameter and we store snapshots of the state variables at select time steps $\mathtt{I}_\mathrm{s} \subset \{1,\dots,J_{\max}\}$; then, we use this piece of information to build a ROM for the state; then, during the online stage, we query the ROM for the same value of the parameter considered in the offline stage.

The solution reproduction problem is of little practical interest; however, it represents the first step towards the implementation of an effective ROM for the parametric problem. Note that during the offline stage we store the state variables in a subset of the time steps and we do not store internal variables: this choice is motivated by the fact that for practical problems memory constraints might prevent the storage of all snapshots; in addition, internal variables might not be computed explicitly by available HF codes.

3.1.1 | Data compression

We resort to POD based on the method of snapshots (cf. Ref.[28]) to generate the ROB $\underline{Z}$. Given the snapshots $\{\underline{U}^{(j)}_{\mathrm{hf},\mu}\}_{j\in\mathtt{I}_\mathrm{s}} = \{\underline{U}^{(k)}\}_{k=1}^K$, $K = |\mathtt{I}_\mathrm{s}|$, we define the Gramian matrix $\mathbf{C} \in \mathbb{R}^{K,K}$ such that $\mathbf{C}_{k,k'} = (\underline{U}^k, \underline{U}^{k'})$; then, we define the POD eigenpairs

$$\mathbf{C}\widetilde{\boldsymbol{\zeta}}_n = \lambda_n\widetilde{\boldsymbol{\zeta}}_n, \quad \lambda_1 \geq \lambda_2 \geq \dots \lambda_K \geq 0;$$

finally, we define the POD modes

$$\underline{\zeta}_n := \sum_{k=1}^{K} \left(\widetilde{\zeta}_n\right)_k \underline{U}_k, \quad n = 1, \dots, N.$$

The reduced space size N can be chosen according to the energy criterion:

$$N := \min\left\{ M \,:\, \sum_{n=1}^{M} \lambda_n \geq (1 - tol_{\text{POD}}^2) \sum_{i=1}^{K} \lambda_i \right\}, \tag{8}$$

for some user-defined tolerance $tol_{\text{POD}} > 0$. Note that the POD modes depend on the choice of the inner product $(\cdot, \cdot)$: we discuss the choice of $(\cdot, \cdot)$ for the THM problem considered in this paper in section 4.

3.1.2 | Hyper-reduction

We denote by $\widehat{\mathbf{R}}_\mu^{\text{hf}}(\cdot)$ and $\widehat{\mathbf{R}}_\mu^{\text{eq}}(\cdot)$ the algebraic reduced residuals associated with the HF and empirical quadrature rules, such that

$$\begin{cases} \left(\widehat{\mathbf{R}}_\mu^{\text{hf}}\left(\boldsymbol{\alpha};\, \boldsymbol{\beta}, \underline{\mathbf{W}}'\right)\right)_n := \mathcal{R}_\mu^{\text{hf}}\left(\underline{\mathbf{Z}}\,\boldsymbol{\alpha},\, \underline{\mathbf{Z}}\,\boldsymbol{\beta},\, \underline{\mathbf{W}}_\mu^\star,\, \underline{\mathbf{W}}',\, \underline{\zeta}_n\right), \quad n = 1, \dots, N, \\ \left(\widehat{\mathbf{R}}_\mu^{\text{eq}}\left(\boldsymbol{\alpha};\, \boldsymbol{\beta}, \underline{\mathbf{W}}'\right)\right)_n := \mathcal{R}_\mu^{\text{eq}}\left(\underline{\mathbf{Z}}\,\boldsymbol{\alpha},\, \underline{\mathbf{Z}}\,\boldsymbol{\beta},\, \underline{\mathbf{W}}_\mu^\star,\, \underline{\mathbf{W}}',\, \underline{\zeta}_n\right), \quad n = 1, \dots, N, \end{cases}$$

where $\boldsymbol{\alpha}, \boldsymbol{\beta} \in \mathbb{R}^N$, $\underline{\mathbf{W}}' \in \mathbb{R}^{n_{\text{q}}, N_{\text{e}}, D_{\text{int}}}$, and $\underline{\mathbf{W}}_\mu^\star = \underline{\mathbf{W}}_\mu^\star\left(\boldsymbol{\alpha}, \boldsymbol{\beta}; \underline{\mathbf{W}}'\right)$ is obtained by substituting in $(4)_3$. We further introduce the Jacobians $\mathbf{J}_\mu^{\text{hf}}(\cdot), \mathbf{J}_\mu^{\text{eq}}(\cdot)$ such that

$$\left(\mathbf{J}_\mu^{\text{hf}}(\boldsymbol{\alpha}; \boldsymbol{\beta}, \underline{\mathbf{W}}')\right)_{n,n'} := \frac{\partial}{\partial \alpha_{n'}} \left(\widehat{\mathbf{R}}_\mu^{\text{hf}}\left(\boldsymbol{\alpha}; \boldsymbol{\beta}, \underline{\mathbf{W}}'\right)\right)_n, \quad \left(\mathbf{J}_\mu^{\text{eq}}(\boldsymbol{\alpha}; \boldsymbol{\beta}, \underline{\mathbf{W}}')\right)_{n,n'} := \frac{\partial}{\partial \alpha_{n'}} \left(\widehat{\mathbf{R}}_\mu^{\text{eq}}\left(\boldsymbol{\alpha}; \boldsymbol{\beta}, \underline{\mathbf{W}}'\right)\right)_n,$$

for $n, n' = 1, \dots, N$. We observe that the computation of the Jacobian involves the derivatives with respect to the constitutive laws in $\underline{\mathcal{F}}^{\text{hf}}$; we further observe that the residuals $\widehat{\mathbf{R}}_\mu^{\text{hf}}(\cdot)$ and $\widehat{\mathbf{R}}_\mu^{\text{eq}}(\cdot)$ satisfy

$$\widehat{\mathbf{R}}_\mu^{\text{hf}}\left(\boldsymbol{\alpha}; \boldsymbol{\beta}, \underline{\mathbf{W}}'\right) = \mathbf{G}\left(\boldsymbol{\alpha}; \boldsymbol{\beta}, \underline{\mathbf{W}}'\right) \boldsymbol{\rho}^{\text{hf}}, \quad \widehat{\mathbf{R}}_\mu^{\text{eq}}\left(\boldsymbol{\alpha}; \boldsymbol{\beta}, \underline{\mathbf{W}}'\right) = \mathbf{G}\left(\boldsymbol{\alpha}; \boldsymbol{\beta}, \underline{\mathbf{W}}'\right) \boldsymbol{\rho}^{\text{eq}}, \tag{9}$$

where $\mathbf{G} \in \mathbb{R}^{N, N_{\text{e}}}$ can be explicitly derived using the same approach as in Ref.[8] and $\boldsymbol{\rho}^{\text{hf}} = [1, \dots, 1]^T$.

As in Ref.[6], we reformulate the problem of finding the sparse weights $\boldsymbol{\rho}^{\text{eq}} \in \mathbb{R}^{N_{\text{e}}}$ as the problem of finding a vector $\boldsymbol{\rho}^{\text{eq}}$ such that:

1. the number of nonzero entries in $\boldsymbol{\rho}^{\text{eq}}$, which we denote by $\|\boldsymbol{\rho}^{\text{eq}}\|_0$, is as small as possible;
2. the entries of $\boldsymbol{\rho}^{\text{eq}}$ are non-negative;
3. (*constant-function constraint*) the constant function is integrated accurately: $\left|\sum_{k=1}^{N_{\text{e}}} \rho_k^{\text{eq}} |\mathtt{D}_k| - |\Omega|\right| \ll 1$;
4. (*manifold accuracy constraint*) the empirical and hf residuals are close at operating conditions:

$$\left\| \left(\mathbf{J}_\mu^{\text{hf}}(\boldsymbol{\alpha}_{\text{train}}^{(j)}, \boldsymbol{\alpha}_{\text{train}}^{(j)}; \underline{\mathbf{W}}_{\text{train}}^{(j-1)})\right)^{-1} \left(\widehat{\mathbf{R}}_\mu^{\text{hf}}\left(\boldsymbol{\alpha}_{\text{train}}^{(j)}, \boldsymbol{\alpha}_{\text{train}}^{(j)}; \underline{\mathbf{W}}_{\text{train}}^{(j-1)}\right) - \widehat{\mathbf{R}}_\mu^{\text{eq}}\left(\boldsymbol{\alpha}_{\text{train}}^{(j)}, \boldsymbol{\alpha}_{\text{train}}^{(j)}; \underline{\mathbf{W}}_{\text{train}}^{(j-1)}\right)\right) \right\|_2 \ll 1, \tag{10}$$

   for $j \in \mathtt{I}_{\text{s}}$ and for suitable choices of $\{\boldsymbol{\alpha}_{\text{train}}^{(j)}\}_j$ and $\{\underline{\mathbf{W}}_{\text{train}}^{(j)}\}_j$ that are discussed at the end of the section.

We observe that a similar problem was already introduced in Refs.[4,9]. Compared to these works, we here add the constant-function constraint that is found to improve the accuracy of the weights when the integrals are close to zero due to the cancellation of the function to be integrated in different parts of the domain (cf. Ref.[6]).

Exploiting (9), we can restate the previous requirements as a sparse representation problem:

$$\text{find } \boldsymbol{\rho}^{\text{eq}} \in \arg\min_{\boldsymbol{\rho} \in \mathbb{R}^{N_{\text{e}}}} \|\boldsymbol{\rho}\|_0 \text{ s.t. } \begin{cases} \boldsymbol{\rho} \geq \mathbf{0} \\ \|\mathbf{C}\boldsymbol{\rho} - \mathbf{b}\|_* \leq \delta, \end{cases} \tag{11}$$

for a suitable choices of the matrix $\mathbf{C}$, the vector $\mathbf{b}$, the norm $\|\cdot\|_*$, and the tolerance δ. Since the optimization problem (11) is NP-hard, several authors have proposed computational methods to find approximate solutions to (11) in polynomial time. To provide concrete references, Ref.[6] considers a ℓ^1 relaxation of (11) with $\|\cdot\|_\star = \|\cdot\|_{\ell^\infty}$, and resorts to linear programming to find

an approximate solution; here, following Farhat et al.[4], we approximate the solution to (11) by solving the inexact non-negative least squares (NNLS) problem

$$\min_{\boldsymbol{\rho}\in\mathbb{R}^{N_e}} \|\mathbf{C}\boldsymbol{\rho}-\mathbf{b}\|_2 \text{ s.t. } \boldsymbol{\rho}\geq\mathbf{0}. \tag{12}$$

A thorough comparison between the reduced quadrature approaches in Ref.[4] and Ref.[6] is beyond the scope of this paper; we refer to Ref.[29] for a detailed analysis of the performance of NNLS and a comparison with LP for a stochastic sparse representation problem with Gaussian disturbances.

In this work, we rely on the Matlab function `lsqnonneg` that implements the Greedy algorithm proposed in Ref.[30] and takes as input the matrix $\mathbf{C}$, the vector $\mathbf{b}$, and a tolerance tol_{eq}:

$$\boldsymbol{\rho}^{\text{eq}} = \texttt{lsqnonneg}(\mathbf{C},\mathbf{b},tol_{\text{eq}}).$$

The same algorithm to find the sparse weights $\boldsymbol{\rho}^{\text{eq}}$ given the matrices $\mathbf{C},\mathbf{b}$ has been first considered in Ref.[4]: for large-scale problems, a parallelised extension of the algorithm was introduced and successfully applied to hyper-reduction in Ref.[31].

Remark 2. The presence of internal variables complexifies the application of EQ procedures. Indeed, the problem formulation in Equation (4) (and Equation (31) for the specific problem of interest) shows the dependence of the residual on state and internal variables both at the current time and at the previous time step. Therefore, in order to compute the entries of $\mathbf{C},\mathbf{b}$ associated with (10), we should prescribe the triplets $\left\{\left(\boldsymbol{\alpha}^{(j)}_{\text{train}},\boldsymbol{\alpha}^{(j-1)}_{\text{train}},\underline{\mathbf{W}}^{(j-1)}_{\text{train}}\right)\right\}_{j\in\mathtt{I}_s}$: knowledge of the primary and internal variables at time j and $j-1$ for $j\in\mathtt{I}_s$ is thus necessary to construct residuals at each time step.

A first option, which was considered in Ref.[9], is to store state and internal variables $\{\underline{U}^{(j)}_{\text{hf}},\underline{U}^{(j-1)}_{\text{hf}},\underline{W}^{(j-1)}_{\text{hf}}\}$ at all select time steps $j\in\mathtt{I}_s$. This choice might lead to very large offline memory costs — which scale with $\left(n_{\text{q}}N_{\text{e}}D_{\text{int}}+2\mathcal{N}D_{\text{eq}}\right)|\mathtt{I}_s|$ — and it might require modifications to the HF solver, but it does not require the solution to the ROM with HF quadrature.

An alternative approach, which is considered in this work, is to use HF data to build the ROB for the state variables, solve the ROM (7) with HF quadrature to obtain $\{\widehat{\boldsymbol{\alpha}}^{(j)}_{\text{hf},\mu},\widehat{\underline{\mathbf{W}}}^{(j)}_{\text{hf},\mu}\}_j$, and then set $\boldsymbol{\alpha}^{(j)}_{\text{train}}=\widehat{\boldsymbol{\alpha}}^{(j)}_{\text{hf},\mu}$ and $\underline{\mathbf{W}}^{(j)}_{\text{train}}=\widehat{\underline{\mathbf{W}}}^{(j)}_{\text{hf},\mu}$. This choice contributes to reduce offline memory costs and might also avoid modifications to the HF solver; however, it increases offline computational costs. In the numerical results (cf. Table 5), we report computational costs of ROM solves based on HF and empirical quadrature.

We emphasize that the other pieces of our approach — Galerkin projection, POD-Greedy algorithm, time-averaged residual indicator — can cope with both strategies. The decision should thus be based on the particular software architecture considered and on the design constraints.

3.2 | Parametric problem

In order to extend our methodology to parametric problems, we should address two challenges. First, we should explore the parameter domain $\mathcal{P}$ in an efficient way; second, we should devise a compression strategy to combine information from different parameters.

In this work we propose an adaptive strategy based on an inexpensive error indicator described in section 3.2.2. Our point of departure is the POD-Greedy algorithm proposed in Ref.[18]. Algorithm 2 summarises the procedure: the procedure takes as input a discretisation of $\mathcal{P}$, Ξ_{train}, a tolerance tol_{loop} for the outer greedy loop, a tolerance tol_{pod} for the data compression step, and the maximum number of greedy iterations $N_{\text{count,max}}$ — we here prescribe the termination condition based on the error indicator; we refer to the pMOR literature for other termination conditions.

We observe that the algorithm depends on several building blocks. The FE solver

$$\left[\{\underline{\mathbf{U}}^{(j)}_{\text{hf},\mu}\}_{j\in\mathtt{I}_s}\right] = \texttt{FE-solve}(\mu)$$

takes as input the vector of parameters and returns the snapshot set associated with the sampling times $\mathtt{I}_s\subset\{1,\dots,J_{\max}\}$ (without saving internal variables, as pointed out in Remark 2). The data compression routine

$$\left[\underline{Z}',\ \lambda'\right] = \texttt{data-compression}\left(\underline{Z},\ \lambda,\{\underline{\mathbf{U}}^{(j)}_{\text{hf},\mu^\star}\}_{j\in\mathtt{I}_s},(\cdot,\cdot),tol_{\text{pod}}\right)$$

takes as input the current ROB and the POD eigenvalues $\lambda=[\lambda_1,\dots,\lambda_N]^T$, and returns the updated ROB $\underline{Z}'$ and the updated eigenvalues λ'; finally, we observe that construction of the ROM comprises both the construction of the Galerkin ROM and of the error indicator. In the remainder of this section, we discuss each element of the procedure.

Algorithm 2 POD-Greedy algorithm

Require: $\Xi_{\text{train}} = \{\mu^{(k)}\}_{k=1}^{n_{\text{train}}}$, tol_{loop}, tol_{pod}, $N_{\text{count,max}}$.

$\mathcal{Z} = \emptyset$, $\lambda = \emptyset$, $\mu^\star = \mu^{(1)}$.
for $n_{\text{count}} = 1, \dots, N_{\text{count,max}}$ **do**
  $\left[\{\underline{\mathbf{U}}^{(j)}_{\text{hf},\mu^\star}\}_{j\in \mathtt{I}_s}\right] = \texttt{FE-solve}(\mu^\star)$;
  $\left[\underline{Z},\ \lambda\right] = \texttt{data-compression}(\underline{Z},\ \lambda, \{\underline{\mathbf{U}}^{(j)}_{\text{hf},\mu^\star}\}_{j\in \mathtt{I}_s}, (\cdot,\cdot), tol_{\text{pod}})$; ▷ section 3.2.1.
  Construct the ROM with error indicator. ▷ section 3.2.3.
  for $j = 1 : n_{\text{train}}$ **do**
    Solve the ROM (7) for $\mu = \mu^{(k)}$ and compute Δ_μ.
  end for
  $\mu^\star = \arg\max_{\mu\in\Xi_{\text{train}}} \Delta_\mu$ ▷ Greedy search
  if $\Delta_{\mu^\star} < tol_{\text{loop}}$ **then**, ▷ Termination condition
    `break`,
  end if.
end for
  return ROB $\underline{Z}$ and ROM: $\mu \in \mathcal{P} \mapsto \{\widehat{\boldsymbol{\alpha}}^{(j)}_\mu\}_{j=1}^{J_{\max}}$.

3.2.1 | Data compression

We consider two different data compression strategies: a hierarchical POD (H-POD) and a hierarchical approximate POD (HAPOD). Both techniques have been considered in several previous works: we refer to Ref.[32, section 3.5] for H-POD and to Ref.[33] for HAPOD; HAPOD is also related to incremental singular value decomposition in linear algebra[34]. Here, we review the two approaches for completeness. We denote by $\Pi_{\mathcal{Z}} : \mathcal{X}_{\text{hf}} \to \mathcal{Z}$ the orthogonal projection operator on $\mathcal{Z} \subset \mathcal{X}_{\text{hf}}$; furthermore, we introduce notation

$$\left[\underline{Z},\ \lambda\right] = \texttt{POD}\left(\{\underline{U}^{(k)}\}_{k=1}^{K}, (\cdot,\cdot), tol_{\text{pod}}\right)$$

to refer to the application of POD to the snapshot set $\{\underline{U}^{(k)}\}_{k=1}^{K}$, with inner product $(\cdot,\cdot)$, and tolerance tol_{pod} (cf. (8)), with $\underline{Z} = [\underline{\zeta}_1, \dots, \underline{\zeta}_N]$, $\|\underline{\zeta}_n\| = 1$, $\lambda = [\lambda_1, \dots, \lambda_N]^T$, and $\lambda_1 \geq \lambda_2 \dots \geq \lambda_N$.

Given $\underline{Z}$ and the snapshots $\{\underline{U}^{(j)}_{\text{hf},\mu^\star}\}_j$ H-POD considers the update:

$$\underline{Z}' = \left[\underline{Z}, \underline{Z}^{\text{new}}\right], \quad \underline{Z}^{\text{new}} = \texttt{POD}\left(\{\Pi_{\mathcal{Z}^\perp}\underline{U}^{(j)}_{\text{hf},\mu^\star}\}_j, (\cdot,\cdot), tol_{\text{pod}}\right). \tag{13a}$$

Note that the approach does not require to input the POD eigenvalues λ from the previous iterations. We observe that the approach leads to a sequence of nested spaces — that is, the updated ROB contains the ROB of the previous iteration — and it returns an orthonormal basis of the reduced space. In our experience, the choice of the tolerance tol_{pod} is extremely challenging: since (8) depends on the relative energy content of the snapshot set, the update (13a) with fixed tolerance tol_{pod} might lead to an excessively large (resp., small) number of modes when $\max_j \|\underline{U}^{(j)}_{\text{hf},\mu^\star} - \Pi_{\mathcal{Z}}\underline{U}^{(j)}_{\text{hf},\mu^\star}\|$ is small (resp., large). For this reason, we propose to choose the number of new modes N^{new} using the criterion:

$$N^{\text{new}} := \min\left\{ M \ :\ \max_{j\in\mathtt{I}_s} \frac{\|\Pi_{(\mathcal{Z}\oplus\mathcal{Z}^{\text{new}}_M)^\perp}\underline{U}^{(j)}_{\text{hf},\mu^\star}\|}{\|\underline{U}^{(j)}_{\text{hf},\mu^\star}\|} \leq tol_{\text{pod}},\ \ \mathcal{Z}^{\text{new}}_M = \text{span}\{\underline{\zeta}^{\text{new}}_m\}_{m=1}^{M} \right\}. \tag{13b}$$

Note that this choice enforces that the in-sample relative projection error is below a certain threshold for all snapshots computed during the greedy iterations.

HAPOD considers the update

$$[\underline{Z}', \lambda'] = \texttt{POD}\left(\{\underline{U}^{(j)}_{\text{hf},\mu^\star}\}_j \cup \{\lambda_n\underline{\zeta}_n\}_{n=1}^{N}, (\cdot,\cdot), tol_{\text{pod}}\right). \tag{14}$$

Note that the approach (14) does not in general lead to hierarchical (nested) spaces. As discussed in Ref.[33, section 3.3], which refers to (14) as to *distributed HAPOD*, it is possible to relate the performance of the reduced space obtained using HAPOD to the

Algorithm 3 Online solution and residual computations

Initial state and internal variables; set $\widehat{\mathbf{R}}_\mu^{\text{avg}} = \mathbf{0}$.
for $j = 1, \dots, J_{\max}$ **do**
  Compute $\widehat{\boldsymbol{\alpha}}_\mu^{(j)}$ by solving (7b).
  Compute $\left(\widehat{\underline{\mathbf{W}}}_\mu^{(j)}\right)_{:,k,:}$ for all $k \in \mathtt{I}_{\text{eq,r}}$ using $(7\text{b})_2$.
  Assemble $\widehat{\mathbf{R}}_\mu^{(j)} \in \mathbb{R}^M$ such that $\left(\widehat{\mathbf{R}}_\mu^{(j)}\right)_m = \mathcal{R}_\mu^{\text{eq,r}}\left(\widehat{\underline{U}}_\mu^{(j)}, \widehat{\underline{U}}_\mu^{(j-1)}, \widehat{\underline{W}}_\mu^{(j)}, \widehat{\underline{W}}_\mu^{(j-1)}, \underline{\psi}_m\right)$ for $m = 1, \dots, M$.
  Update $\widehat{\mathbf{R}}_\mu^{\text{avg}} = \widehat{\mathbf{R}}_\mu^{\text{avg}} + (t^{(j)} - t^{(j-1)})\widehat{\mathbf{R}}_\mu^{(j)}$.
end for
  return $\{\widehat{\boldsymbol{\alpha}}_\mu^{(j)}\}_j$ and $\Delta_\mu = \|\widehat{\mathbf{R}}_\mu^{\text{avg}}\|_2$

performance of the POD space associated with the snapshot set $\{\underline{U}_{\text{hf},\mu^\star,n}^{(j)} \ : \ n = 1, \dots, N_{\text{count,max}}, \ j \in \mathtt{I}_{\text{s}}\}$: we refer to the above-mentioned paper for a thorough discussion.

3.2.2 | Time-averaged error indicator

We define the trajectories $\mathbb{U} = \{\underline{U}^{(j)}\}_{j=1}^{J_{\max}}$ and $\mathbb{W} = \{\underline{W}^{(j)}\}_{j=1}^{J_{\max}}$; given the pair $(\mathbb{U}, \mathbb{W})$, we define the time-average residual:

$$\mathcal{R}_{\text{avg},\mu}^{\text{hf}}\left(\mathbb{U}, \mathbb{W}, \underline{V}\right) := \sum_{j=1}^{J_{\max}} (t^{(j)} - t^{(j-1)}) \, \mathcal{R}_\mu^{\text{hf}}\left(\underline{U}^{(j)}, \underline{U}^{(j-1)}, \underline{W}^{(j)}, \underline{W}^{(j-1)}, \underline{V}\right), \quad \forall \, \underline{V} \in \mathcal{X}_{\text{hf},0}, \tag{15}$$

and the error indicator

$$\Delta_\mu^{\text{hf}}(\mathbb{U}, \mathbb{W}) = \sup_{\underline{V} \in \mathcal{X}_{\text{hf},0}} \frac{\mathcal{R}_{\text{avg},\mu}^{\text{hf}}\left(\mathbb{U}, \mathbb{W}, \underline{V}\right)}{\|\underline{V}\|}. \tag{16}$$

The indicator (16) is expensive to evaluate since it relies on hf quadrature and it requires the computation of the supremum over all elements of $\mathcal{X}_{\text{hf},0}$: following Ref.[35], we consider the hyper-reduced error indicator

$$\Delta_\mu(\mathbb{U}, \mathbb{W}) = \sup_{\underline{V} \in \mathcal{Y}} \frac{\mathcal{R}_{\text{avg},\mu}^{\text{eq,r}}\left(\mathbb{U}, \mathbb{W}, \underline{V}\right)}{\|\underline{V}\|}, \tag{17}$$

where $\mathcal{Y} \subset \mathcal{X}_{\text{hf},0}$ is an M-dimensional empirical test space, while $\mathcal{R}_{\text{avg},\mu}^{\text{eq,r}}$ is defined by replacing $\mathcal{R}_\mu^{\text{hf}}$ in (15) with a suitable sparse weighted residual of the form (7a), defined over the elements $\mathtt{I}_{\text{eq,r}} \subset \{1, \dots, N_{\text{e}}\}$.

Given the ROM solution $(\widehat{\mathbb{U}}_\mu, \widehat{\mathbb{W}}_\mu)$, the test space $\mathcal{Y}$ should guarantee that

$$\sup_{\underline{V} \in \mathcal{Y}} \frac{\mathcal{R}_{\text{avg},\mu}^{\text{hf}}\left(\widehat{\mathbb{U}}_\mu, \widehat{\mathbb{W}}_\mu, \underline{V}\right)}{\|\underline{V}\|} \approx \sup_{\underline{V} \in \mathcal{X}_{\text{hf},0}} \frac{\mathcal{R}_{\text{avg},\mu}^{\text{hf}}\left(\widehat{\mathbb{U}}_\mu, \widehat{\mathbb{W}}_\mu, \underline{V}\right)}{\|\underline{V}\|}, \quad \forall \mu \in \mathcal{P}, \tag{18}$$

which implies that $\mathcal{Y}$ should be an approximation of the space of Riesz elements $\mathcal{M}_{\text{test}} := \{\underline{\widehat{\psi}}_\mu \ : \ \mu \in \mathcal{P}\}$ with

$$\left(\underline{\widehat{\psi}}_\mu, \underline{V}\right) = \mathcal{R}_{\text{avg},\mu}^{\text{hf}}\left(\widehat{\mathbb{U}}_\mu, \widehat{\mathbb{W}}_\mu, \underline{V}\right), \quad \forall \, \underline{V} \in \mathcal{X}_{\text{hf},0}. \tag{19}$$

On the other hand, the empirical quadrature rule should ensure that

$$\mathcal{R}_{\text{avg},\mu}^{\text{eq,r}}\left(\widehat{\mathbb{U}}_\mu, \widehat{\mathbb{W}}_\mu, \underline{\psi}_m\right) \approx \mathcal{R}_{\text{avg},\mu}^{\text{hf}}\left(\widehat{\mathbb{U}}_\mu, \widehat{\mathbb{W}}_\mu, \underline{\psi}_m\right), \quad \forall \, \mu \in \mathcal{P}, \ m = 1, \dots, M, \tag{20}$$

where $\underline{\psi}_1, \dots, \underline{\psi}_M$ is an orthonormal basis of $\mathcal{Y}$.

In our implementation, we compute the error indicator during the time iterations — as opposed to after having computed the whole solution trajectory. Algorithm 3 provides the complete online solution and residual indicator computations. We find that computation of Δ_μ requires to compute the internal variables $\widehat{\mathbb{W}}_\mu$ in the elements $\mathtt{I}_{\text{eq}} \cup \mathtt{I}_{\text{eq,r}}$ at each time iteration (cf. (7b)), and it requires to store the trial ROB $\underline{Z}$ in $\{\mathtt{D}_k \ : \ k \in \mathtt{I}_{\text{eq}} \cup \mathtt{I}_{\text{eq,r}}\}$ and the test basis $\underline{Y} = [\underline{\psi}_1, \dots, \underline{\psi}_M]$ in $\{\mathtt{D}_k \ : \ k \in \mathtt{I}_{\text{eq,r}}\}$.

Algorithm 4 Construction of the ROM

1: **for** $\mu \in \Xi^\star$ **do**
2: Solve the ROM with hf quadrature and compute $\mathbf{C}_\mu$ and $\mathbf{R}_\mu^{\text{avg,un}}$.
3: **end for**
4: Assemble $\mathbf{C} = \begin{bmatrix} \mathbf{C}_{\tilde{\mu}^{(1)}} \\ \vdots \\ \mathbf{C}_{\tilde{\mu}^{(n_{\text{rom}})}} \\ \mathbf{c}^T \end{bmatrix} \in \mathbb{R}^{K\cdot N\cdot n_{\text{rom}}, N_{\text{e}}}$ and set $\boldsymbol{\rho}^{\text{eq}} = \texttt{lsqnonneg}(\mathbf{C}, \mathbf{C}\boldsymbol{\rho}^{\text{hf}}, tol_{\text{eq}})$.
5: Compute the Riesz representers $\{\underline{\widehat{\psi}}_\mu\}_{\mu\in\Xi_\star}$ using (19).
6: Define the empirical test space $\mathcal{Y} = \text{span}\{\underline{\psi}_m\}_{m=1}^M$ as $[\{\underline{\psi}_m\}_{m=1}^M] = \texttt{POD}\left(\{\underline{\widehat{\psi}}_\mu\}_{\mu\in\Xi_\star}, (\cdot,\cdot), tol_{\text{pod,res}}\right)$.
7: Assemble $\mathbf{G} = \begin{bmatrix} \mathbf{G}_{\tilde{\mu}^{(1)}} \\ \vdots \\ \mathbf{G}_{\tilde{\mu}^{(n_{\text{rom}})}} \\ \mathbf{c}^T \end{bmatrix} \in \mathbb{R}^{M\cdot n_{\text{rom}}, N_{\text{e}}}$ and set $\boldsymbol{\rho}^{\text{eq,r}} = \texttt{lsqnonneg}(\mathbf{G}, \mathbf{G}\boldsymbol{\rho}^{\text{hf}}, tol_{\text{eq,r}})$.

Several authors (e.g., Ref. [18]) have considered the time-discrete $L^2(0,T_{\text{f}};\mathcal{X}'_{\text{hf},0})$ residual indicator

$$\Delta_\mu^{\text{hf},2}(\mathbb{U},\mathbb{W}) = \sqrt{\sum_{j=1}^{J_{\max}} (t^{(j)} - t^{(j-1)}) \left(\sup_{\underline{V}\in\mathcal{X}_{\text{hf},0}} \frac{\mathcal{R}_\mu^{\text{hf}}\left(\underline{U}^{(j)}, \underline{U}^{(j-1)}, \underline{W}^{(j)}, \underline{W}^{(j-1)}, \underline{V}\right)}{\|\underline{V}\|} \right)^2}. \tag{21}$$

We observe that we could apply the same ideas considered in this section to devise an hyper-reduced counterpart of the residual indicator (21). However, we find that the test space $\mathcal{Y}$ and the empirical quadrature rule should be accurate for all parameters and for all time steps: as a result, the resulting test space $\mathcal{Y}$ might be significantly higher dimensional and the quadrature rule might be significantly less sparse, for the desired accuracy. For this reason, in this work, we investigate the effectivity of the time-averaged error indicator (17).

3.2.3 | ROM construction

In order to devise an actionable ROM, we should discuss (i) the choice of the EQ rule $\boldsymbol{\rho}^{\text{eq}}$, (ii) the choice of the test space $\mathcal{Y}$ and of the EQ rule $\boldsymbol{\rho}^{\text{eq,r}}$ in (17). In view of the presentation of the computational procedure, we define the ROM solution with hf quadrature $(\widehat{\mathbb{U}}_\mu^{\text{hf}}, \widehat{\mathbb{W}}_\mu^{\text{hf}})$; we denote by $\mathbf{C}_\mu \in \mathbb{R}^{K\cdot N, N_{\text{e}}}$ the EQ matrix associated with the manifold accuracy constraints in (10) for $\mu \in \mathcal{P}$ (cf. section 3.1.2); we further define the vector $\mathbf{c} = [|\mathtt{D}_1|, \dots, |\mathtt{D}_{N_{\text{e}}}|]^T$ associated with the constant function accuracy constraint. Given the test reduced basis $\underline{\psi}_1, \dots, \underline{\psi}_M$, we define $\mathbf{G}_\mu^{\text{r}} \in \mathbb{R}^{M, N_{\text{e}}}$ such that

$$\left(\mathbf{G}_\mu^{\text{r}}\boldsymbol{\rho}_{\text{hf}}\right)_m = \mathcal{R}_{\text{avg},\mu}^{\text{eq,r}}\left(\widehat{\mathbb{U}}_\mu^{\text{hf}}, \widehat{\mathbb{W}}_\mu^{\text{hf}}, \underline{\psi}_m\right), \quad \forall\, \mu\in\mathcal{P},\ m = 1,\dots,M. \tag{22}$$

We further define the unassembled average residual $\mathbf{R}_\mu^{\text{avg,un}} \in \mathbb{R}^{n_{\text{lp}}, N_{\text{e}}, D_{\text{eq}}}$: we observe that $\mathbf{R}_\mu^{\text{avg,un}}$ might be employed to build the FE residual and ultimately compute the Riesz representers $\underline{\widehat{\psi}}_\mu$ in (19), and also, given $\mathcal{Y}$, to compute $\mathbf{G}_\mu^{\text{r}}$.

We focus on the construction of the ROM at the n_{c}-th iteration of the POD Greedy algorithm. We define $\Xi^\star = \{\tilde{\mu}^{(j)}\}_{j=1}^{n_{\text{rom}}} = \{\mu^{\star,(i)}\}_{i=1}^{n_{\text{c}}} \cup \{\tilde{\mu}^{(j)}\}_{j=1}^{n_{\text{train,eq}}}$, where $\mu^{\star,(1)}, \dots, \mu^{\star,(n_{\text{c}})}$ are the parameters sampled by the greedy algorithm and $\tilde{\mu}^{(1)}, \dots, \tilde{\mu}^{(n_{\text{train,eq}})}$ are independent identically distributed samples from the uniform distribution over $\mathcal{P}$. Algorithm 4 summarises the computational procedure as implemented in our code. The test space $\mathcal{Y}$ is built using POD as in Ref. [35], while the EQ weights $\underline{\rho}_{\text{eq,r}}$ are obtained using the non-negative least-squares method.

	SI unit	description
$\underline{u}$	m	solid displacement
p_{w}	Pa	water pressure
T	K	temperature

TABLE 1 primary variables

	SI unit	label
ρ_{w}	$\mathrm{kg}\cdot\mathrm{m}^{-3}$	water density
φ	%	Eulerian porosity
h_{w}	$\mathrm{J}\cdot\mathrm{Kg}^{-1}$	mass enthalpy of water
Q	Pa	non-convected heat
$\underline{M}_{\mathrm{w}}$	$\mathrm{kg}\cdot\mathrm{m}^{-2}\cdot\mathrm{s}^{-1}$	mass flux
m_{w}	$\mathrm{kg}\cdot\mathrm{m}^{-3}$	mass input

TABLE 2 dependent variables

	SI unit	value
$\bar{t}$	s	$3.15\cdot10^{7}$
$\bar{H}$	m	77.3
σ_0	Pa	$11.3\cdot10^{6}$
ρ_0	$\mathrm{kg}\cdot\mathrm{m}^{-3}$	2450
T_{ref}	K	297.5
ΔT	K	30

TABLE 3 characteristic constants

4 | THM MODEL PROBLEM

In this section we illustrate the non-dimensional mathematical formulation and the numerical discretisation of the THM system considered in this work. We assume that the solid undergoes small displacements and that soil is fully-saturated in water. We resort to a Lagrangian formulation for the solid, and to an Eulerian formulation for the fluid.

4.1 | Preliminary definitions

We first introduce the state variables and the internal variables. The state variables are denoted as $\underline{U}_\mu$ in the continuous formulation in Equation (1), and their FE approximation as $\underline{\mathbf{U}}_\mu^{\mathrm{hf}}$ in the high-fidelity discretisation in Equation (4). For the specific problem of interest, $\underline{U} = [\underline{u}^{\mathrm{T}}, p_{\mathrm{w}}, T]^{\mathrm{T}}$: the state variables represent solid displacement, water pressure and temperature and are reported in Table 1; the internal variables $\underline{W} = [\rho_{\mathrm{w}}, \varphi, h_{\mathrm{w}}, Q, \underline{M}_{\mathrm{w}}^{\mathrm{T}}, m_{\mathrm{w}}]^{\mathrm{T}}$ represent dependent physical quantities and are illustrated in Table 2, together with the corresponding SI units.

We denote the Cauchy stress tensor by $\underline{\underline{\sigma}}$[Pa], and we define the volumetric deformation $\epsilon_{\mathrm{V}} = tr(\underline{\underline{\epsilon}})$ where $\underline{\underline{\epsilon}}$ is the strain tensor: $\underline{\underline{\epsilon}} = \nabla_{\mathrm{s}}\underline{u} = \frac{1}{2}\left(\nabla\underline{u} + \nabla\underline{u}^{T}\right)$. We also provide in Table 3 the characteristic parameters that we use for the non-dimensionalisation.

4.1.1 | Geometry configuration

The computational domain is shown in Figure 1(a). The geological repositories, modelled as boundary conditions, are depicted in red at the bottom of the domain, in the case of two activated alveoli. In the vertical (x_2) direction, the domain is split into

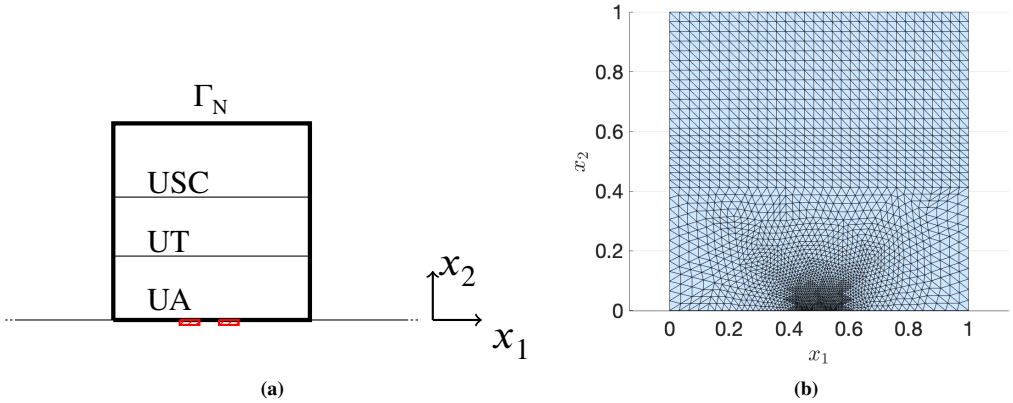

(a) (b)

FIGURE 1 geometric configuration: (a) the non-dimensional domain (b) the mesh. The size of each alveoulus is equal to $l_Q = 3.09$ [m], while the distance between consecutive alveoli is equal to $l = 6.18$ [m].

three layers: a clay layer denoted as UA ("*unité argilleuse*"), a transition layer UT ("*unité de transition*") and a silt-carbonate layer USC ("*unité silto-carbonatée*").
In Figure 1(b) the finite element grid is shown. The number of degrees of freedom for the first state component (solid displacement) is $\mathcal{N}^{\mathrm{u}} = 40430$, while for water pressure and temperature is $\mathcal{N}^{\mathrm{p}} = \mathcal{N}^{\mathrm{t}} = 9045$. The grid is refined in the proximity of the alveoli to better capture the relevant features of the solution. We consider a $\mathrm{p} = 3$ FE discretisation for the displacement component, and a $\mathrm{p} = 2$ FE discretisation for both pressure and temperature.

4.2 | Mathematical problem

We first state the equilibrium equations – the superscripts $(\cdot)^{\mathrm{m}}$, $(\cdot)^{\mathrm{n}}$,$(\cdot)^{\mathrm{t}}$ refer to quantities associated with the mechanical, hydraulic and thermal behaviours, respectively. Then, we present the constitutive laws that are considered and finally we present the boundary conditions. To clarify the presentation, we report in Table 4 the parameters that enter in the constitutive laws.

We denote by $\underline{F}_{\mathrm{m}} = -\frac{g}{\gamma}\underline{e}_2$ (where $\gamma = \frac{\sigma_0}{\rho_0 H}$) the mechanical force with g defined in Table 4 and we specify that $\underline{n}$ (resp. $\underline{t}$) is the unitary outward normal (resp. tangential) vector in the domain depicted in Figure 1(a); then we introduce the equilibrium of mechanical forces:

$$\begin{cases} -\nabla \cdot \underline{\underline{\sigma}} = \rho \underline{F}_{\mathrm{m}} & \text{in } \Omega, \\ \underline{\underline{\sigma}}\,\underline{n} = \underline{g}_{\mathrm{m,N}} & \text{on } \Gamma_{\mathrm{N}}, \\ \underline{u} \cdot \underline{n} = 0 & \text{on } \partial\Omega \setminus \Gamma_{\mathrm{N}}, \\ (\underline{\underline{\sigma}}\,\underline{n}) \cdot \underline{t} = 0 & \text{on } \partial\Omega \setminus \Gamma_{\mathrm{N}}, \end{cases} \tag{23a}$$

where Γ_{N} is depicted in Figure 1(a). The Neumann datum $\underline{g}_{\mathrm{m,N}}$ is given by $\underline{g}_{\mathrm{m,N}} = -\underline{e}_2$. The stress tensor is linked to the primary and internal variables by the linear law

$$\underline{\underline{\sigma}} = 2\mu \nabla_{\mathrm{s}} \underline{u} + \left(\lambda\, \nabla \cdot \underline{u} - (2\mu + 3\lambda)\alpha_{\mathrm{s}} T - b p_{\mathrm{w}}\right) \mathbb{1}, \tag{23b}$$

where the Lamé constants μ', λ satisfy

$$\mu' = \frac{E}{2(1+\nu)},$$
$$\lambda = \frac{E\nu}{(1+\nu)(1-2\nu)},$$

and E and ν are introduced in Table 4.

We state the mass conservation of water as follows

$$\begin{cases} \partial_t m_{\mathrm{w}} + \nabla \cdot \underline{\underline{M}}_{\mathrm{w}} = 0 \ \text{in}\,\Omega \\ \underline{\underline{M}}_{\mathrm{w}} \cdot \underline{n} = 0 \qquad\qquad \text{on}\,\partial\Omega \end{cases} \tag{24a}$$

where the muss flux $\underline{\underline{M}}_{\mathrm{w}}$ is given by the Darcy law

$$\underline{\underline{M}}_{\mathrm{w}} = -\gamma \left(\nabla p_{\mathrm{w}} - \rho_{\mathrm{w}} \underline{F}_{\mathrm{m}} \right), \tag{24b}$$

and

$$\gamma = \rho_{\mathrm{w}} \frac{\kappa_{\mathrm{w}}\, \sigma_0\, \bar{t}}{\rho_0 \mu_{\mathrm{w},0}\, \bar{H}^2} \exp\left(-\frac{1808.5}{T_{\mathrm{ref}} + \overline{\Delta T}\, T} \right). \tag{24c}$$

Finally we consider the energy balance:

$$\begin{cases} h_{\mathrm{w}} \partial_t m_{\mathrm{w}} + \partial_t \mathcal{Q} + \nabla \cdot \left(h_{\mathrm{w}} \underline{\underline{M}}_{\mathrm{w}} + \underline{q} \right) - \underline{\underline{M}}_{\mathrm{w}} \cdot \underline{F}_{\mathrm{m}} = \Theta \ \text{in}\,\Omega \\ \left(h_{\mathrm{w}} \underline{\underline{M}}_{\mathrm{w}} + \underline{q} \right) \cdot \underline{n} = g_{\mathrm{t,N}} \qquad\qquad \text{on}\,\partial\Omega \end{cases} \tag{25a}$$

where $\mathcal{Q}$ is the non-convective heat, $\underline{q}$ is the thermal flux and is given by the Fick law

$$\underline{q} = -\Lambda \nabla T, \tag{25b}$$

with $\Lambda = \mathrm{diag}(\lambda_1, \lambda_2)$. If we denote by $\Gamma_{\mathrm{al}} \subset \partial\Omega$ the region associated with the alveoli, $g_{t,N}$ is equal to

$$g_{t,N} = \frac{P_{\mathrm{t}} n_c \bar{t}}{l_Q \bar{H}^2 \sigma_0} \exp\left(-t/\tau \right) \mathbb{1}_{\Gamma_{\mathrm{al}}} = C_{\mathrm{al}} \exp\left(-t/\tau \right) \mathbb{1}_{\Gamma_{\mathrm{al}}}, \tag{26}$$

where n_c [%] is the density of the radioactive waste stock in each alveolus (equal to 45 anisters), $P_{\mathrm{t}} = 31.4$ [W] is the unitary termic power at the initial time, $l_Q = 3.09$ [m] is the size of each alveolus, σ_0, $\bar{H}$, $\bar{t}$ are introduced in Table 3 and $\tau = \frac{\bar{t}}{\log(0.112)}$ [s] is a characteristic decay time.

$$\begin{cases} \dfrac{d\rho_{\mathrm{w}}}{\rho_{\mathrm{w}}} = \dfrac{dp_{\mathrm{w}}}{K_{\mathrm{w}}} - 3\alpha_{\mathrm{w}} dT & (27a) \\ \dfrac{d\varphi}{b - \varphi} = d\epsilon_{\mathrm{V}} - 3\alpha_{\mathrm{s}} dT + \dfrac{dp_{\mathrm{w}}}{K_{\mathrm{s}}}, & (27b) \\ dh_{\mathrm{w}} = C_{\mathrm{w}}^{\mathrm{p}}\, dT + (\beta_h^{\mathrm{p}} - 3\alpha_{\mathrm{w}} T) \dfrac{dp_{\mathrm{w}}}{\rho_{\mathrm{w}}}, & (27c) \\ \delta\mathcal{Q} = \left(\beta_{\mathcal{Q}}^{\epsilon} + 3\alpha_{\mathrm{s}} K_0\, T \right) d\epsilon_{\mathrm{V}} - \left(\beta_{\mathcal{Q}}^{\mathrm{p}} + 3\alpha_{\mathrm{w,m}} T \right) dp_{\mathrm{w}} + C_{\epsilon}^0\, dT, & (27d) \\ m_{\mathrm{w}} = \rho_{\mathrm{w}}(1 + \epsilon_{\mathrm{V}})\, \varphi - \rho_{\mathrm{w}}^0 \varphi^0 & (27e) \end{cases}$$

Here, we have $\beta_h^p = 1 - 3\alpha_{\mathrm{w}} T_{\mathrm{ref}}$, $\beta_{\mathcal{Q}}^{\epsilon} = 3\alpha_{\mathrm{s}} K_0 T_{\mathrm{ref}}$, $\beta_{\mathcal{Q}}^p = 3\alpha_{\mathrm{w,m}} T_{\mathrm{ref}}$.
The parameters in (27a)-(27e) are defined in Table 4.

4.2.1 | Initial conditions

To set the initial conditions, we consider the case of deactivated repositories: therefore, we set thermal flux equal to zero and we set a constant temperature $T_0 = T_{\mathrm{ref}}$ in Ω, where the reference temperature is defined in Table 3. We aim at finding the initial values of the primary variables $\underline{u}$ and p_{w} that correspond to the equilibium solutions of a preliminary problem: here, the Neumann boundary condition for the energy equation is zero, that is, $g_{\mathrm{t,N}} = 0$, and temperature is costant and equal to the reference value T_{ref} (in Table 3).
We then seek $\underline{u}_0$, $p_{\mathrm{w},0}$ such that the initial solution vector $\underline{U}_0 = [\underline{u}_0^{\mathrm{T}}, p_{\mathrm{w}}, T_0]^{\mathrm{T}}$ satisfies the equilibrium equations (23a), (24a) and (25a) with thermal flux $g_{\mathrm{t,N}}$ equal to 0 on the domain boundary $\partial\Omega$. Towards this end, we first observe that (27a) reduces to

$$\frac{d\rho_{\mathrm{w}}}{\rho_{\mathrm{w}}} = \frac{dp_{\mathrm{w}}}{K_{\mathrm{w}}} \tag{28}$$

	SI unit	description	reference value	formula
g	$\mathrm{m}\cdot\mathrm{s}^{-2}$	gravity acceleration	9.81	
			$11.4\cdot10^9$ UA	
E	Pa	Young's modulus	$12.3\cdot10^9$ UT	
			$20\cdot10^9$ USC	
ν	%	Poisson's ratio	0.3	
μ	Pa	Lamé parameter,		$\frac{E}{2(1+\nu)}$
λ	Pa	Lamé parameter		$\frac{E\nu}{(1+\nu)(1-2\nu)}$
b	%	Biot coefficient	0.6	
α_s	K^{-1}	solid thermal expansion coefficient	$1.28\cdot10^{-5}$	
α_0	K^{-1}	expansion coefficient	$1.28\cdot10^{-5}$	
κ_w	m^2	intrinsic permeability of porous medium	10^{-21}	
μ_w	$\mathrm{MPa}\cdot\mathrm{s}$	dynamic viscosity		$\mu_\mathrm{w}=\mu_{\mathrm{w},0}\exp(\frac{1808.5}{T})$
$\mu_{\mathrm{w},0}$	$\mathrm{MPa}\cdot\mathrm{s}$	dynamic viscosity coefficient	$2.1\cdot10^{-12}$	
K_s	Pa	bulk modulus of the solid		
K_w	Pa	bulk modulus of water	$2\cdot10^9$	$K_\mathrm{s}=\frac{E}{3(1-2\nu)}$
C_w^p	$\mathrm{J}\cdot\mathrm{kg}^{-1}\cdot\mathrm{K}^{-1}$	heat capacity at constant pressure	4180	
K_0	Pa	drained bulk modulus		$K_0=(1-b)K_\mathrm{s}$
α_w	K^{-1}	thermal expansion coefficient of water		$\alpha_\mathrm{w}=9.52\cdot10^{-5}\log(T-273)-2.19\cdot10^{-4}$
$\alpha_{\mathrm{w,m}}$		dilation coefficient		
			537 UA	
C_σ^s	$\mathrm{J\,kg}^{-1}\cdot\mathrm{K}$	specific heat at constant stress	603 UT	
			640 USC	
			2450 UA	
ρ^0	$\mathrm{Kg}\cdot\mathrm{m}^{-3}$	porous medium initial density	2450 UT	
			2500 USC	
ρ_w^0	$\mathrm{Kg}\cdot\mathrm{m}^{-3}$	initial water density	10^3	
			0.25 UA	
φ^0	%	initial Eulerian porosity	0.21 UT	
			0.19 USC	
h_w^0	$\mathrm{m}^2\cdot\mathrm{s}^{-2}$	initial water enthalpy		$h_\mathrm{w}^0=\frac{p_\mathrm{w}^0-p_\mathrm{atm}}{\rho_\mathrm{w}^0}$
ρ_s	$\mathrm{Kg}\cdot\mathrm{m}^{-3}$	density ratio		$\rho_\mathrm{s}=\frac{\rho^0-\rho_\mathrm{w}^0\varphi^0}{1-\varphi^0}$
C_ϵ^0	$\mathrm{Pa}\cdot\mathrm{K}^{-1}$	specific heat at constant deformation		$C_\epsilon^0=(1-\varphi)\rho_s C_\sigma^s+\varphi\rho_w C_w^p-9TK_0\alpha_\mathrm{s}^2$
Λ		thermic conductivity tensor		$\Lambda=\mathrm{diag}(\lambda_1,\lambda_2)$
			1.5 UA	
λ_1	$\mathrm{Wm}^{-1}\mathrm{K}^{-1}$	thermic conductivity component	1.5 UT	
			1.3 USC	
			1 UA	
λ_2	$\mathrm{Wm}^{-1}\mathrm{K}^{-1}$	thermic conductivity component	1 UT	
			1.3 USC	
Θ	$\mathrm{Pa}\cdot\mathrm{s}^{-1}$	volumetric heat sources		

TABLE 4 parameters of the constitutive laws. Layers UA, UT, USC are depicted in Figure 1 (a).

that brings to $p_\mathrm{w}=\rho_{-\infty}\exp\left(\frac{1}{K_\mathrm{w}}(p_\mathrm{w}-p_{-\infty})\right)$. If we assume that $\rho_\mathrm{w}=\rho_{-\infty}=\rho_{\mathrm{w},0}$, we find $p_\mathrm{w}=p_{-\infty}$; furthermore, by susbstituting these assumptions into the hydraulic equilibrium equation we find

$$p_{\mathrm{w},0}(x,y)=p_{\mathrm{w,top}}+\rho_{\mathrm{w},0}g(1-y) \tag{29}$$

where $p_{\mathrm{w,top}}$ is a datum for water pressure that is defined at the top boundary of the domain $(0,1)\times\{1\}$. Finally, we search for $\underline{u}_0$ as the solution to the equilibrium equation of mechanical forces:

$$\int_\Omega 2\mu\,\nabla_{\mathrm{s}}\,\underline{u}_0\ :\ \nabla_{\mathrm{s}}\,\underline{v}\ +\ \lambda(\nabla\cdot\underline{u}_0)(\nabla\cdot\underline{v}) - bp_{\mathrm{w},0}\,\nabla\cdot\underline{v}\ -\ \rho^0\underline{F}_{\mathrm{m}}\cdot\underline{v}\,dx = \int_{\Gamma_{\mathrm{N}}}\underline{g}_{\mathrm{m,N}}\cdot\underline{v}\,dx, \tag{30}$$

for all $\underline{v}\in\mathcal{X}^{\mathrm{u}}_{\mathrm{hf}}$, such that $\underline{v}\cdot\underline{n}|_{\partial\Omega\setminus\Gamma_{\mathrm{N}}}=0$.

4.3 | Finite element formulation

We resort to an implicit Euler time discretisation scheme, with $J_{\max}=100$ uniform time steps; the superscript $(\cdot)^+$ refers to the new solution (at the current time step j, for $j=1,...,J_{\max}$), while $(\cdot)^-$ refers to the solution at the previous time steps:

$$\begin{cases}
\displaystyle\int_\Omega 2\mu\,\nabla_{\mathrm{s}}\,\underline{u}^+\ :\ \nabla_{\mathrm{s}}\,\underline{v}\ +\ \left(\lambda\nabla\cdot\underline{u}^+\ -\ (2\mu+3\lambda)\,\alpha_{\mathrm{s}}T^+ - bp^+_{\mathrm{w}}\right)\nabla\cdot\underline{v}\ -\ \left(\rho^0+m^+_{\mathrm{w}}\right)\underline{F}_{\mathrm{m}}\cdot\underline{v}\,dx \\
\qquad\qquad = \displaystyle\int_{\Gamma_{\mathrm{N}}}\underline{g}^+_{\mathrm{m,N}}\cdot\mathbf{v}\,dx; \\
\displaystyle\int_\Omega \frac{1}{\Delta t}(m^+_{\mathrm{w}}-m^-_{\mathrm{w}})\,\psi\ +\ \gamma^+(\nabla p^+_{\mathrm{w}}-\rho^+_{\mathrm{w}}\underline{F}_{\mathrm{m}})\cdot\nabla\psi\,dx\ =0; \\
\displaystyle\int_\Omega\left(\left(\frac{h_{\mathrm{w}}}{\Delta t}(m^+_{\mathrm{w}}-m^-_{\mathrm{w}})\ +\ \frac{1}{\Delta t}(\mathcal{Q}^+-\mathcal{Q}^-)\ +\ \gamma^+(\nabla p^+_{\mathrm{w}}-\rho^+_{\mathrm{w}}\underline{F}_{\mathrm{m}})\cdot\underline{F}_{\mathrm{m}}\right)\xi\ -\ \left(-h^-_{\mathrm{w}}(\nabla p^+_{\mathrm{w}}-\rho^+_{\mathrm{w}}\underline{F}_{\mathrm{m}})\ +\ \underline{q}\right)\cdot\nabla\xi\right. \\
\qquad\qquad = \displaystyle\int_\Omega\Theta^+\xi\,dx\ -\ \int_{\partial\Omega} g^+_{\mathrm{t,N}}\,\xi\,dx;
\end{cases} \tag{31}$$

for all $\underline{v}\in\mathcal{X}^{\mathrm{u}}_{\mathrm{hf}}$ such that $\underline{v}\cdot\underline{n}|_{\partial\Omega\setminus\Gamma_N}=0$, $\psi\in\mathcal{X}^{\mathrm{p}}_{\mathrm{hf}}$, $\xi\in\mathcal{X}^{\mathrm{t}}_{\mathrm{hf}}$, where

$$\begin{cases}
\rho^+_{\mathrm{w}}\ =\ \rho^-_{\mathrm{w}}\exp\left(\dfrac{p^+_{\mathrm{w}}-p^-_{\mathrm{w}}}{K_{\mathrm{w}}}\ -\ 3\alpha_{\mathrm{w}}(T^+-T^-)\right); \\
\varphi^+ = b\ -\ (b-\varphi^-)\exp\left(-(\epsilon^+_{\mathrm{V}}-\epsilon^-_{\mathrm{V}})+3\alpha_0(T^+-T^-)\ -\ \dfrac{1}{K_s}\,(p^+_{\mathrm{w}}-p^-_{\mathrm{w}})\right); \\
h^+_{\mathrm{w}} = h^-_{\mathrm{w}}\ +\ C^{\mathrm{p}}_{\mathrm{w}}\,(T^+-T^-)\ +\ \dfrac{\beta^{\mathrm{p}}_h-3\alpha_{\mathrm{w}}T^+}{\rho^+_{\mathrm{w}}}\,\left(p^+_{\mathrm{w}}-p^-_{\mathrm{w}}\right); \\
\mathcal{Q}^+ = \mathcal{Q}^-\ +\ \left(\beta^{\epsilon}_{\mathcal{Q}}+3\alpha_{\mathrm{s}}K_0\,\dfrac{1}{2}(T^++T^-)\right)\left(\epsilon^+_{\mathrm{V}}-\epsilon^-_{\mathrm{V}}\right)\ -\left(\beta^{\mathrm{p}}_{\mathcal{Q}}+3\alpha^+_{\mathrm{w,m}}\dfrac{1}{2}(T^++T^-)\right)\left(p^+_{\mathrm{w}}\ -\ p^-_{\mathrm{w}}\right) \\
\qquad\qquad\qquad\qquad\qquad\qquad\qquad\qquad + C^{0,+}_{\epsilon}\,(T^+-T^-); \\
m^+_{\mathrm{w}} = \rho^+_{\mathrm{w}}(1+\epsilon^+_{\mathrm{V}})\,\varphi^+ - \rho^0_{\mathrm{w}}\,\varphi^0.
\end{cases} \tag{32}$$

We remark that integrals in system (31)-(32) depend on internal variables at the current times $t^{(j)}$ and at the previous times $t^{(j-1)}$, for $j=1,...,J_{\max}$: this model problem thus fits in the general problem introduced in Eq. (4).

4.4 | Choice of the norm

We equip the FE space $\mathcal{X}_{\mathrm{hf}}$ with the weighted inner product

$$(\underline{U},\underline{U}') = \frac{1}{\lambda_{\mathrm{u}}}\sum_{d=1}^{2}(\underline{u}_d,\underline{u}'_d)_{H^1(\Omega)} + \frac{1}{\lambda_{\mathrm{p}}}(p,p')_{H^1(\Omega)} + \frac{1}{\lambda_{\mathrm{t}}}(T,T')_{H^1(\Omega)}, \tag{33}$$

where the coefficients $\lambda_{\mathrm{u}},\lambda_{\mathrm{p}},\lambda_{\mathrm{t}}$ are the largest eigenvalues of the Gramian matrices $\mathbf{C}^{\mathrm{u}}$, $\mathbf{C}^{\mathrm{p}}$, $\mathbf{C}^{\mathrm{t}}$ associated to displacement, pressure and temperature, respectively. Similarly to Ref.[35], the inner product (33) is motivated by the need for properly taking into account the contributions of displacement, pressure and temperature, which are characterised by different magnitudes and different units.

4.5 | Parametrization

We consider a vector of four parameters: the Young's modulus E and the Poisson's ratio ν in the region UA, the thermic factor τ and the constant C_{al} in (26). For all parameters, we define the parameter domain $\mathcal{P}$ by considering variations of $\pm 15\%$ with respect to the nominal value reported in Table 4.

5 | NUMERICAL RESULTS

We measure performance through the discrete $L^2(0, T_{\text{f}}; \mathcal{X}_{\text{hf}})$ relative error

$$E_\mu := \frac{\sqrt{\sum_{j=1}^{J_{\max}} \left(t^{(j)} - t^{(j-1)}\right) \left\| \underline{U}^{(j)}_{\text{hf},\mu} - \underline{\widehat{U}}^{(j)}_{\mu} \right\|^2}}{\sqrt{\sum_{j=1}^{J_{\max}} \left(t^{(j)} - t^{(j-1)}\right) \| \underline{U}^{(j)}_{\text{hf},\mu} \|^2}} \tag{34}$$

for any $\mu \in \mathcal{P}$. Similarly, we denote by E^{u}_μ, E^{p}_μ and E^{t}_μ the discrete relative $L^2(0, T_{\text{f}}; \mathcal{X}_{\text{hf}})$ errors associated with the estimate of displacement, pressure and temperature, respectively.

5.1 | Solution reproduction problem

We first present numerical results for a fixed configuration of parameters $\bar{\mu} \in \mathcal{P}$ to validate the ROM described in section 3. We consider $\bar{\mu}$ equal to the centroid of $\mathcal{P}$. We perform data compression based on the whole set of snapshots, i.e. $|I_{\text{s}}| = J_{\max} = 100$.

5.1.1 | Data compression: POD

In Figure 2 we compare performance of the global POD based on the weighted inner product $(\cdot, \cdot)$ with the performance of the component-wise POD. More precisely, we define $\underline{Z}$ such that

$$[\underline{Z}, \lambda] = \texttt{POD}\left(\{\underline{U}^{(j)}_{\text{hf},\bar{\mu}}\}_{j \in I_{\text{s}}}, (\cdot, \cdot), tol_{\text{pod}} \right), \tag{35}$$

and we then extract reduced basis associated to the single state variables of interest, that is, we extract the displacement, pressure and temperature components $\underline{Z}^{\text{u}}$, $\underline{Z}^{\text{p}}$, $\underline{Z}^{\text{t}}$.

Then, we denote the "optimal" (in a discrete L^2 sense) spaces

$$[\underline{Z}^{u,\text{opt}}, \lambda^{u,\text{opt}}] = \texttt{POD}\left(\{\underline{u}^{(j)}_{\text{hf},\bar{\mu}}\}_{j \in \mathtt{I}_{\text{s}}}, (\cdot, \cdot)_{H^1}, tol_{\text{pod}} \right); \tag{36}$$

$$[\underline{Z}^{p,\text{opt}}, \lambda^{p,\text{opt}}] = \texttt{POD}\left(\{p^{(j)}_{\text{hf},\bar{\mu}}\}_{j \in \mathtt{I}_{\text{s}}}, (\cdot, \cdot)_{H^1}, tol_{\text{pod}} \right); \tag{37}$$

$$[\underline{Z}^{T,\text{opt}}, \lambda^{T,\text{opt}}] = \texttt{POD}\left(\{T^{(j)}_{\text{hf},\bar{\mu}}\}_{j \in \mathtt{I}_{\text{s}}}, (\cdot, \cdot)_{H^1}, tol_{\text{pod}} \right), \tag{38}$$

that are found through $D_{\text{eq}} - 1$ PODs over displacement, pressure and temperature.

In Figure 2 (a) we show the behaviour of the POD eigenvalues in (35); in Figure 2(b), (c), (d) we compare the relative projection errors associated with $\underline{Z}^{\text{u}}$ and $\underline{Z}^{\text{u,opt}}$, $\underline{Z}^{\text{p}}$, $\underline{Z}^{\text{p,opt}}$ and $\underline{Z}^{\text{t}}$ and $\underline{Z}^{\text{t,opt}}$. We observe that the projection errors are nearly the same for all the three state variables: this obervation suggests to consider a single reduced space to approximate the solution field.

5.1.2 | Hyper-reduction

In Figure 3(a) we show the performance of the Galerkin ROM with and without hyper-reduction. We distinguish between the high-fidelity quadrature rule, abbreviated as HFQ, and the empirical quadrature rule for several tolerances tol_{eq}. We also add as a reference, the relative projection error. Figure 3(b) shows the percentage of selected elements $\frac{\mathtt{Q}}{N_{\text{e}}} \times 100\%$ for the same choices of the tolerance tol_{eq}. We observe that the empirical quadrature procedure is able to significantly reduce the size of the mesh used for online calculations without compromising accuracy. The plateau for $N \gtrsim 14$ is due to the tolerance of the Newton iterative solver.

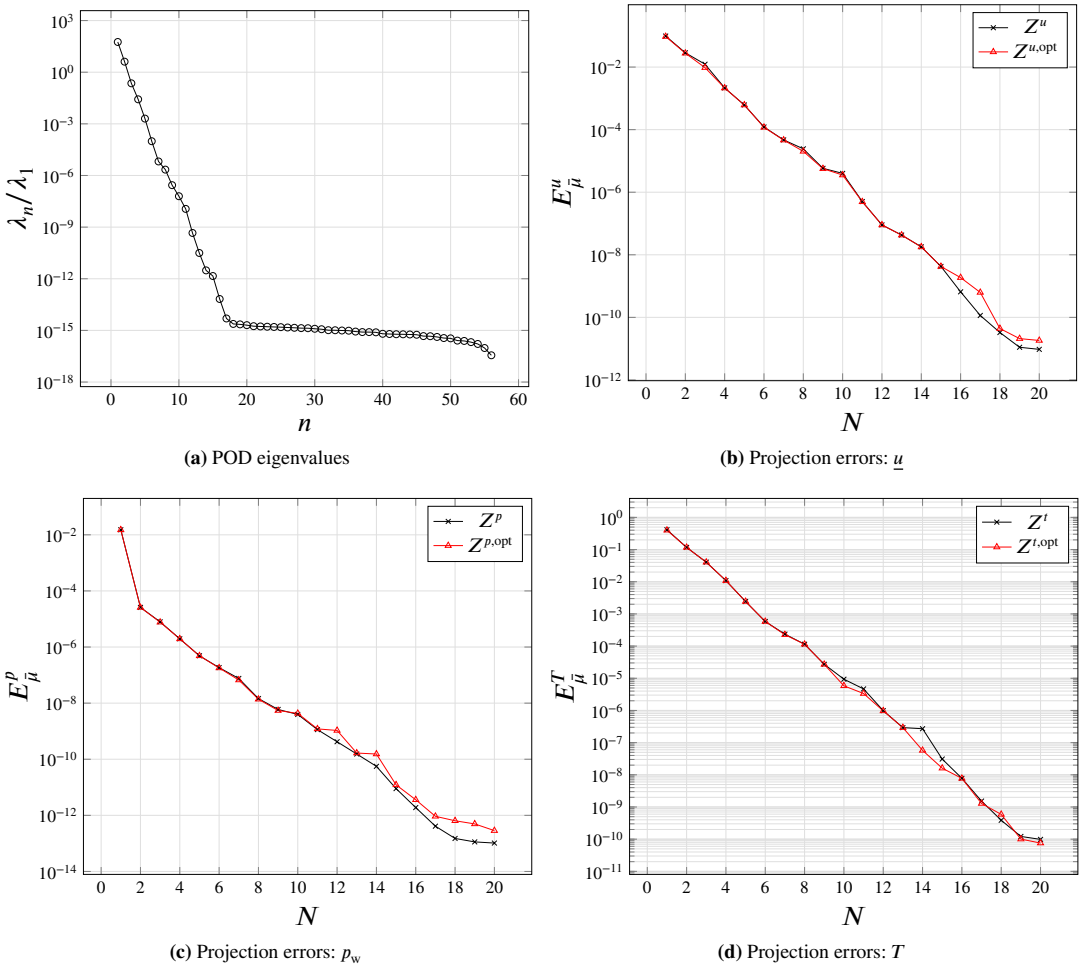

(a) POD eigenvalues

(b) Projection errors: $\underline{u}$

(c) Projection errors: p_w

(d) Projection errors: T

FIGURE 2 solution reproduction problem. (a): exponential decay of POD eigenvalues. (b), (c), (d): projection errors computed through (35) (in black) and (36)-(38)(in red) for increasing numbers of POD modes.

In Figure 4, we show the selected grid elements for two choices of the EQ tolerance value tol_{eq} and for $N = 12$. We observe that the sampled elements are distributed over the whole domain with a slight prevalence of elements in the proximity of the alveoli.

We report in Table 5 the computational costs associated to the solution of system (31)-(32) through the high-fidelity solver and the ROM with high-fidelity quadrature and empirical quadrature, for the solution reproduction problem. We consider a reduced space of size $N = 12$; we also set $tol_{eq} = 10^{-14}$. The values in Table 5 are the computational speedup, that is, speedup $= \frac{\text{HF cost}}{\text{ROM cost}}$ where HF cost is the computational time of solving the high-fidelity solver and ROM cost is the computational time associated to the ROM (we specify in different rows if with HFQ or EQ). The speedup associated to the ROM with high-fidelity quadrature is almost 2 and is more than 50 times lower than the speedup of the hyper-reduced ROM. For this model problem, the cost associated with ROM with HFQ is comparable with the cost of the HF solver. As discussed in Remark 2, the choice of solving a ROM with high-fidelity quadrature significantly increases the offline computation costs.

5.2 | Parametric problem

We present results for the parametric case. We denote by $\Xi_{\text{train}} \subset \mathcal{P}$ the training set used to build the ROM and by $\Xi_{\text{test}} \subset \mathcal{P}$ the test set used to assess performance. Both sets consist of independent identically distributed samples of a uniform distribution in $\mathcal{P}$, with $|\Xi_{\text{train}}| = n_{\text{train}} = 50$ and $|\Xi_{\text{test}}| = n_{\text{test}} = 10$. We also set $tol_{\text{POD}} = 10^{-7}$ in (8) and in (13b) for data compression, and

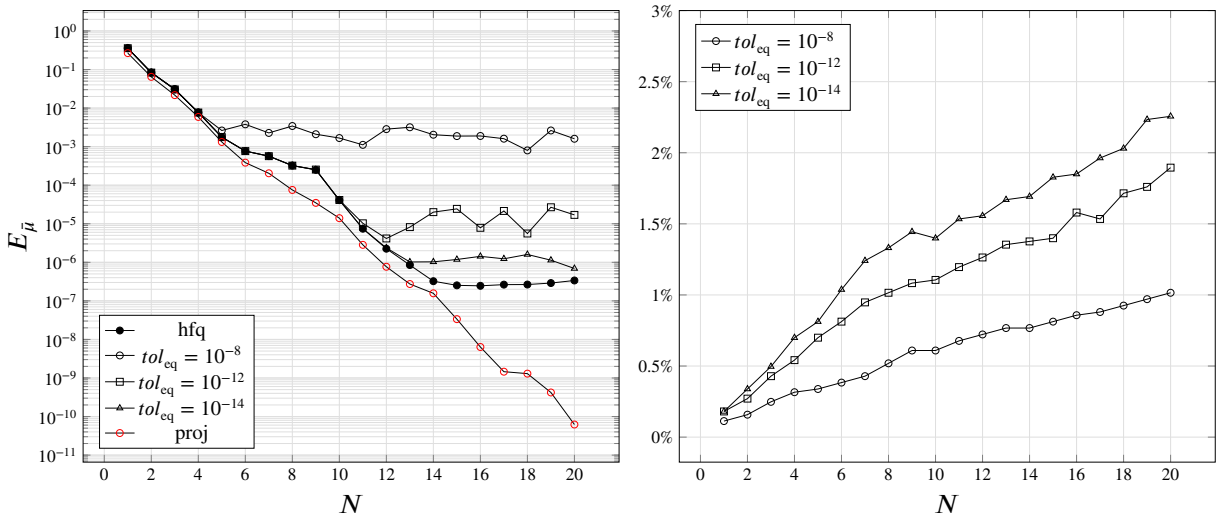

(a) Errors **(b)** Selected elements

FIGURE 3 solution reproduction problem. (a): errors associated to projection error (proj), Galerkin with high-fidelity quadrature (HFQ) and Galerkin with empirical quadrature for several choices of tol_{eq} with respect to the ROM dimension N. (b): percentage of selected elements for several tol_{eq}.

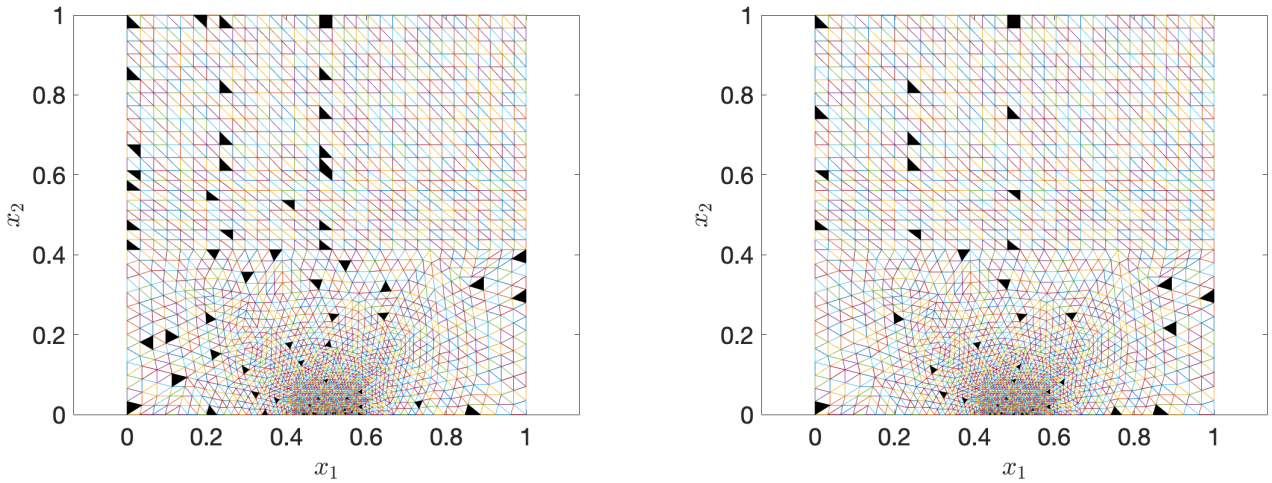

(a) $tol_{\text{eq}} = 10^{-14}$ **(b)** $tol_{\text{eq}} = 10^{-10}$

FIGURE 4 solution reproduction problem. Reduced mesh for two choices of the empirical quadrature tolerance.

we set $tol_{\text{POD,res}} = 10^{-5}$ in (8) for the construction of the empirical test space. We set $I_{\text{s}} \subset \{1, ..., J_{\max}\}$ with $|I_{\text{s}}| = 20$. EQ rules are depicted usign the tolerance $tol_{\text{eq}} = 10^{-12}$ (cf . Algorithm 4).

5.2.1 | Error estimation

In Figure 5 we compare the dual residual and several EQ errors for each parameter μ in the training set Ξ_{train} and for different dimensions of the reduced space that is progressively updated during the execution of the POD-Greedy algorithm. In particular, we show results in two cases: the hierarchical POD-Greedy (H-POD) and the hierarchical approximate POD-Greedy (denoted as HA-POD). Figures 5(a) and 5(b) show for both H-POD and HA-POD to what extent the residual-based error indicator defined

	speedup
HF	1
ROM with HFQ	1.87
ROM with EQ	104.60

TABLE 5 solution reproduction problem: relative computational costs of the ROM with high-fidelity quadrature and empirical quadrature.

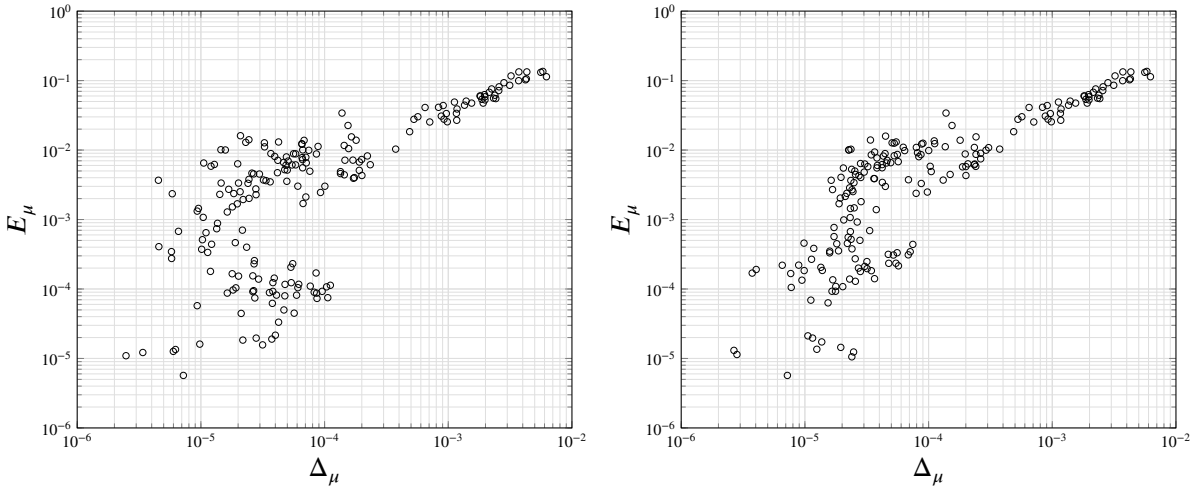

(a) H-POD **(b)** HA-POD

FIGURE 5 parametric problem: correlation between the time-average residual indicator (17) and true relative errors (34).

in (17) is correlated with the relative error (34). We observe that for values of the indicators that are larger than 10^{-3}, correlation is very high, while for smaller values correlation is much weaker.

To provide a a concrete reference, in Figure 6 we investigate the correlation between the relative error (34) and the time-discrete $L^2(0, T_f; \mathcal{X}'_{hf,0})$ residual indicator defined in (21): we observe that the indicator in (21) is significantly more accurate, particularly for small values of the error. As stated in section 3, the residual indicator (21) is considerably more expensive in terms of both memory and computational costs.

5.2.2 | POD-Greedy sampling

In Figures 7 and 8 we show the POD-Greedy algorithm convergence history, for both the hierarchical and approximate hierarchical PODs. At each iteration of the algorithm, until convergence, the error indicator Δ_μ is illustrated with respect to training parameter indices $\mathcal{I}_{train} = \{1, ..., |\Xi_{train}|\}$. At each iteration the selected parameter $\mu^\star$ is marked in red, while the previously selected parameters are marked in green. We also report the dimension of the updated reduced space and the number of sampled elements.

5.2.3 | Prediction tests

In Figure 9, we assess out-of-sample performance of the proposed method. More precisely, we show the behaviour of the maximum relative error (34) over the test set $\max_{\mu \in \Xi_{test}} E_\mu$ for both H-POD Greedy and HA-POD Greedy. To provide a relevant benchmark, we compare results with the H-POD Greedy and HA-POD Greedy algorithms based on the exact errors (strong POD-Greedy). For this particular example, we observe that the proposed method is effective to generate accurate ROMs: in particular, the Greedy procedures based on the time-averaged error indicator are comparable in terms of performance with the corresponding strong POD-Greedy algorithms.

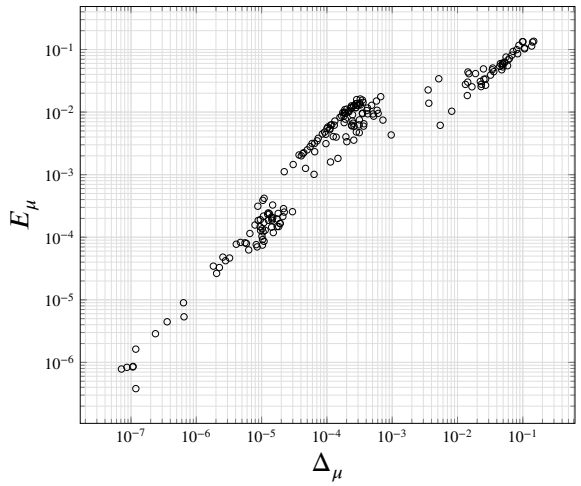

FIGURE 6 parametric problem: correlation between residual indicator (21) and true relative errors 34.

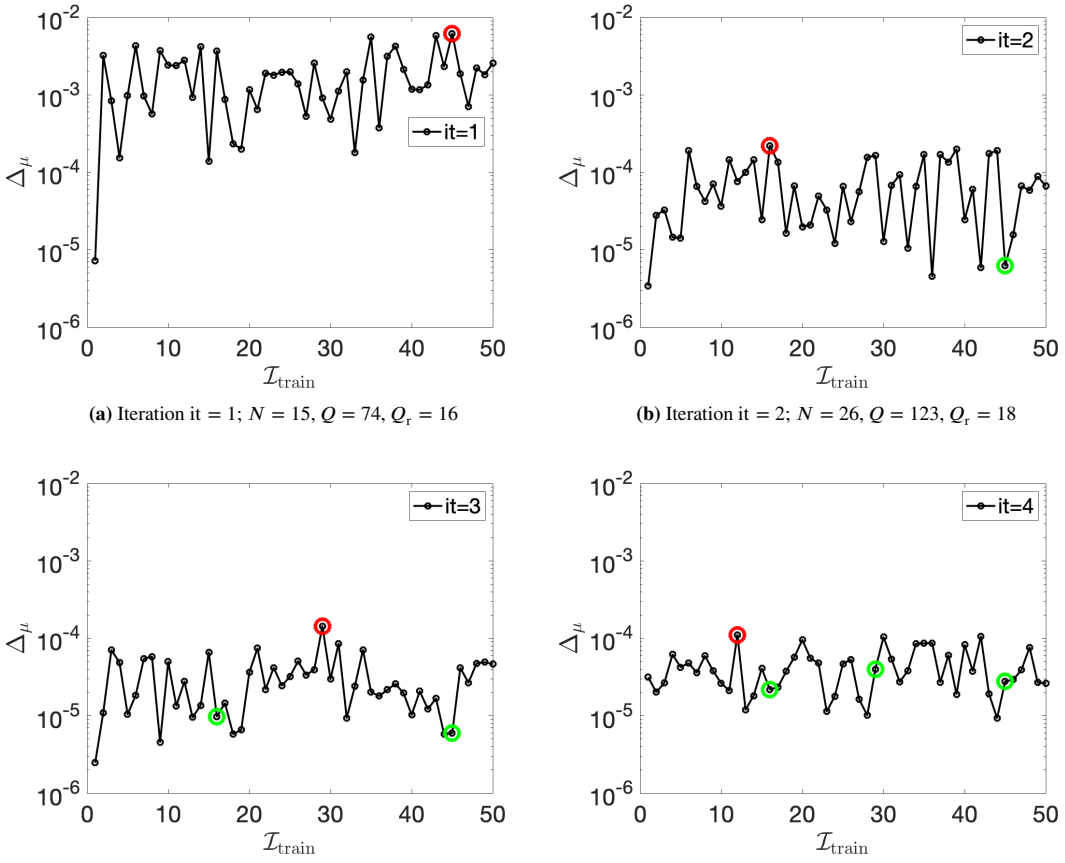

(a) Iteration it $= 1$; $N = 15$, $Q = 74$, $Q_r = 16$

(b) Iteration it $= 2$; $N = 26$, $Q = 123$, $Q_r = 18$

(c) Iteration it $= 3$; $N = 35$, $Q = 155$, $Q_r = 22$

(d) Iteration it $= 4$; $N = 43$, $Q = 169$, $Q_r = 18$

FIGURE 7 parametric problem: POD-Greedy algorithm convergence history in the H-POD case.

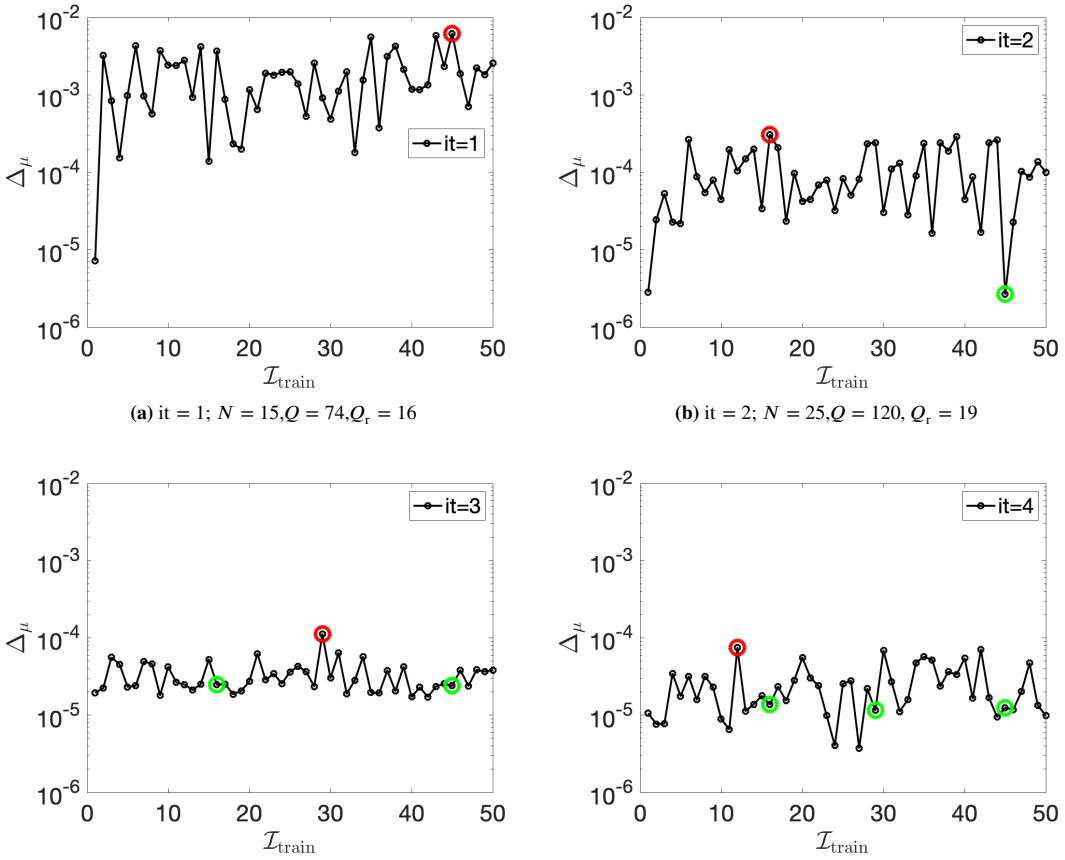

(a) it = 1; $N = 15$,$Q = 74$,$Q_r = 16$

(b) it = 2; $N = 25$,$Q = 120$, $Q_r = 19$

(c) it = 3; $N = 31$,$Q = 135$, $Q_r = 21$

(d) Iteration it = 4; $N = 37$,$Q = 156$, $Q_r = 19$

FIGURE 8 parametric problem: POD-Greedy algorithm convergence history in the HA-POD case.

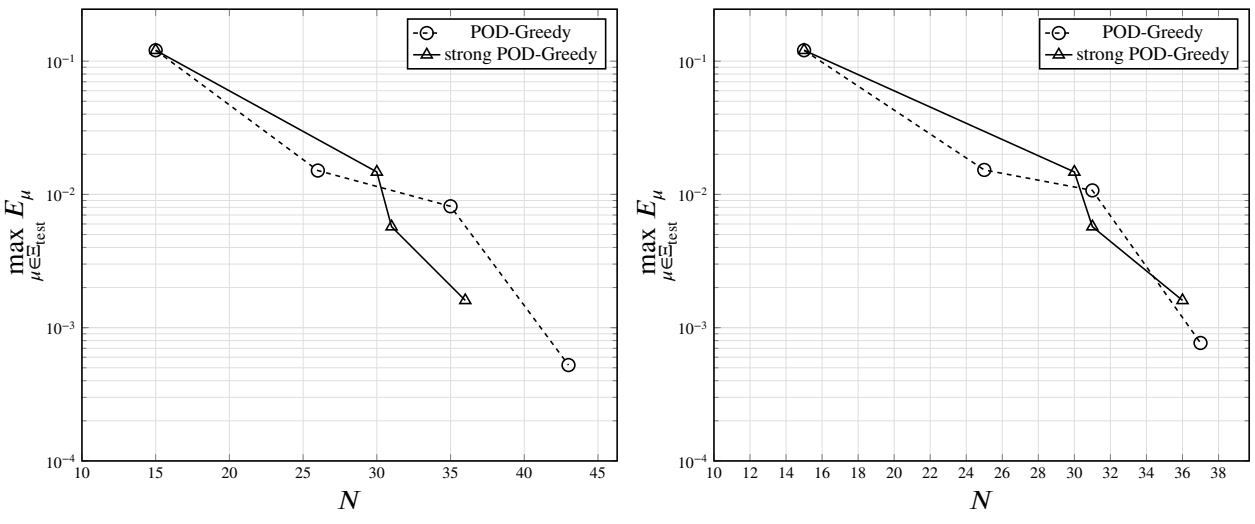

(a) H-POD Greedy

(b) HA-POD Greedy

FIGURE 9 parametric problem:out-of-sample performance of the ROM parametric problem obtained using the POD-Greedy algorithm. Comparison with strong POD Greedy.

6 | CONCLUSIONS

In this work, we developed and numerically validated a model order reduction procedure for a class of problems in nonlinear mechanics, and we successfully applied it to a two-dimensional parametric THM problem that arises in radioactive waste management. We proposed a time-averaged error indicator to drive the offline Greedy sampling, and an empirical quadrature procedure to reduce offline costs.

We aim to extend the approach in several directions. First, we wish to apply our method to other problems of the form (1), to demonstrate the generality of the approach and its relevance for continuum mechanics applications. Second, we wish to combine our approach with domain decomposition methods[36,37,38] to deal with more complex parametrizations and topological changes. Towards this end, we wish to devise effective localised training methods to reduce offline costs and domain decomposition strategies to glue together the solution in different components of the domain.

ACKNOWLEDGMENTS

The authors acknowledge the financial support of Andra (National Agency for Radioactive Waste Management) and thank Dr. Marc Leconte and Dr. Antoine Pasteau (Andra) for fruitful discussions. The authors also acknowledge the support by European Union's Horizon 2020 research and innovation programme under the Marie Sk lodowska-Curie Actions, grant agreement 872442 (ARIA).

Financial disclosure

None reported.

Conflict of interest

The authors declare no potential conflict of interests.

Data availability statement

The data used to support the findings of this work are included within the article. In particular, physical parameters of the THM model can be found in Table 4 (we suggest to see also[39]). Raw numerical data that have been used to generate tables and figures in the paper as well as the Matlab source files are available upon request.

References

1. Hesthaven JS, Rozza G, Stamm B. *Certified reduced basis methods for parametrized partial differential equations*. Springer . 2016.

2. Quarteroni A, Manzoni A, Negri F. *Reduced basis methods for partial differential equations: an introduction*. 92. Springer . 2015.

3. Rozza G, Huynh DBP, Patera AT. Reduced basis approximation and a posteriori error estimation for affinely parametrized elliptic coercive partial differential equations. *Archives of Computational Methods in Engineering* 2007; 15(3): 229–275.

4. Farhat C, Chapman T, Avery P. Structure-preserving, stability, and accuracy properties of the energy-conserving sampling and weighting method for the hyper reduction of nonlinear finite element dynamic models. *International Journal for Numerical Methods in Engineering* 2015; 102(5): 1077–1110.

5. Yano M. Discontinuous Galerkin reduced basis empirical quadrature procedure for model reduction of parametrized nonlinear conservation laws. *Advances in Computational Mathematics* 2019: 1–34.

6. Yano M, Patera AT. An LP empirical quadrature procedure for reduced basis treatment of parametrized nonlinear PDEs. *Computer Methods in Applied Mechanics and Engineering* 2019; 344: 1104–1123.

7. Riffaud S, Bergmann M, Farhat C, Grimberg S, Iollo A. The DGDD method for reduced-order modeling of conservation laws. *Journal of Computational Physics* 2021; 437: 110336.

8. Taddei T, Zhang L. A discretize-then-map approach for the treatment of parameterized geometries in model order reduction. *Computer Methods in Applied Mechanics and Engineering* 2021; 384: 113956.

9. Farhat C, Avery P, Chapman T, Cortial J. Dimensional reduction of nonlinear finite element dynamic models with finite rotations and energy-based mesh sampling and weighting for computational efficiency. *International journal for numerical methods in engineering* 2014.

10. Zahr M, Avery P, Farhat C. A multilevel projection-based model order reduction framework for nonlinear dynamic multiscale problems in structural and solid mechanics. *International journal for numerical methods in engineering* 2017.

11. Barrault M, Maday Y, Nguyen NC, Patera AT. An empirical interpolation method: application to efficient reduced-basis discretization of partial differential equations. *Comptes Rendus Mathematique* 2004; 339(9): 667–672.

12. Chaturantabut S, Sorensen DC. Nonlinear model reduction via discrete empirical interpolation. *SIAM Journal on Scientific Computing* 2010; 32(5): 2737–2764.

13. Ryckelynck D. Hyper-reduction of mechanical models involving internal variables. *International Journal for Numerical Methods in Engineering* 2009; 77(1): 75–89.

14. Carlberg K, Farhat C, Cortial J, Amsallem D. The GNAT method for nonlinear model reduction: effective implementation and application to computational fluid dynamics and turbulent flows. *Journal of Computational Physics* 2013; 242: 623–647.

15. Willcox K. Unsteady flow sensing and estimation via the gappy proper orthogonal decomposition. *Computers & fluids* 2006; 35(2): 208–226.

16. Casenave F, Akkari N, Bordeu F, Rey C, Ryckelynck D. A nonintrusive distributed reduced-order modeling framework for nonlinear structural mechanics-Application to elastoviscoplastic computations. *International journal for numerical methods in engineering* 2018.

17. Hernández J, Caicedo M, Ferrer A. Dimensional hyper-reduction of nonlinear finite element models via empirical cubature. *Computational Methods in Applied Mechanics and Engineering* 2017; 313: 687-722.

18. Haasdonk B, Ohlberger M. Reduced basis method for finite volume approximations of parametrized linear evolution equations. *ESAIM: Mathematical Modelling and Numerical Analysis* 2008; 42(2): 277–302.

19. Haasdonk B. Convergence rates of the POD-greedy method. *ESAIM: Mathematical Modelling and Numerical Analysis* 2013; 47(3): 859–873.

20. Berkooz G, Holmes P, Lumley J. The proper orthogonal decomposition in the analysis of turbulent flows. *Annual review of fluid mechanics* 1993; 25(1): 539–575.

21. Bergmann M, Bruneau CH, Iollo A. Enablers for robust POD models. *Journal of Computational Physics* 2009; 228(2): 516–538.

22. Volkwein S. Model reduction using proper orthogonal decomposition. *Lecture Notes, Institute of Mathematics and Scientific Computing, University of Graz. see math.uni-konstanz.de/numerik/personen/volkwein/teaching/POD-Vorlesung.pdf* 2011; 1025.

23. Fick L, Maday Y, Patera AT, Taddei T. A stabilized POD model for turbulent flows over a range of Reynolds numbers: Optimal parameter sampling and constrained projection. *Journal of Computational Physics* 2018; 371: 214 - 243. doi: https://doi.org/10.1016/j.jcp.2018.05.027

24. Miled B, Ryckelynck D, Cantournet S. A priori hyper-reduction method for coupled viscoelastic–viscoplastic composites. *Computers & Structures* 2013; 119: 95–103.

25. Leuschner M, Fritzen F. Reduced order homogenization for viscoplastic composite materials including dissipative imperfect interfaces. *Mechanics of Materials* 2017; 104: 121–138.

26. Larion Y, Zlotnik S, Massart TJ, Díez P. Building a certified reduced basis for coupled thermo-hydro-mechanical systems with goal-oriented error estimation. *Computational mechanics* 2020; 66(3): 559–573.

27. Granet S. Modélisations THHM. Généralités et algorithmes. https://www.code-aster.org/V2/doc/v9/fr/man_r/r7/r7.01.10.pdf, 2009; .

28. Sirovich L. Turbulence and the dynamics of coherent structures. I. Coherent structures. *Quarterly of applied mathematics* 1987; 45(3): 561–571.

29. Slawski M, Hein M. Sparse recovery by thresholded non-negative least squares. *Advances in Neural Information Processing Systems* 2011: 1926–1934.

30. Lawson CL, Hanson RJ. *Solving least squares problems*. 161. Siam . 1974.

31. Chapman T, Avery P, Collins P, Farhat C. Accelerated mesh sampling for the hyper reduction of nonlinear computational models. *International Journal for Numerical Methods in Engineering* 2017; 109(12): 1623–1654.

32. Haasdonk B. Reduced basis methods for parametrized PDEs–a tutorial introduction for stationary and instationary problems. *Model reduction and approximation: theory and algorithms* 2017; 15: 65.

33. Himpe C, Leibner T, Rave S. Hierarchical approximate proper orthogonal decomposition. *SIAM Journal on Scientific Computing* 2018; 40(5): A3267–A3292.

34. Brand M. Fast online SVD revisions for lightweight recommender systems. In: SIAM. ; 2003: 37–46.

35. Taddei T. An offline/online procedure for dual norm calculations of parameterized functionals: empirical quadrature and empirical test spaces. *Advances in Computational Mathematics* 2019; 45(5-6): 2429–2462.

36. Bergmann M, Ferrero A, Iollo A, Lombardi E, Scardigli A, Telib H. A zonal Galerkin-free POD model for incompressible flows. *Journal of Computational Physics* 2018; 352: 301–325.

37. Kaulmann S, Ohlberger M, Haasdonk B. A new local reduced basis discontinuous Galerkin approach for heterogeneous multiscale problems. *Comptes Rendus Mathematique* 2011; 349(23-24): 1233–1238.

38. Huynh DBP, Knezevic DJ, Patera AT. A static condensation reduced basis element method: approximation and a posteriori error estimation. *ESAIM: Mathematical Modelling and Numerical Analysis* 2013; 47(1): 213–251.

39. Granet S. Modélisations THHM. Généralités et algorithmes. 2009: 1-32.